PNE-1100

PNE-1100

Plowshare civil, industrial and scientific uses for nuclear explosives

UNITED STATES ARMY CORPS OF ENGINEERS

FORT PECK RESERVOIR
MONTANA

PROJECT
PRE-GONDOLA

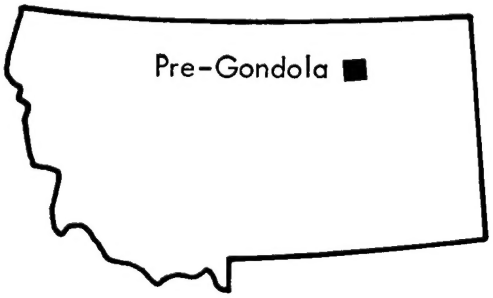

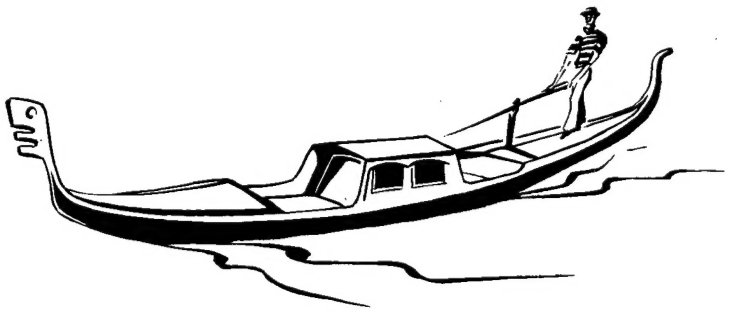

SEISMIC SITE CALIBRATION

LT. COLONEL MAURICE K. KURTZ, JR. LT. BRUCE B. REDPATH

U. S. Army Engineer Nuclear Cratering Group

Livermore, California

U. S. Army Engineer Nuclear Cratering Group
Livermore, California

ISSUED: May 1968

PNE-1100

PROJECT PRE-GONDOLA

SEISMIC SITE CALIBRATION

Lt. Colonel Maurice K. Kurtz, Jr.
Lt. Bruce B. Redpath

U. S. Army Enginner
Nuclear Cratering Group
Livermore, California

January 1968

Abstract

Measurements of intermediate range ground motions and of structural response were made during the Pre-Gondola high explosive cratering experiments at Fort Peck, Montana. Liquid nitromethane charges (1000-lb and 20-ton), emplaced at various depths of burst, and a 140-ton row charge were detonated in the Bearpaw shale, which is a weak, wet clay-shale medium. An additional experiment to validate a charge emplacement concept designed to decouple seismic energy proved inconclusive. All seismic measurements were of particle velocity. Using an inverse power law equation to describe the attenuation of seismic amplitudes with distance, it is found that the amplitudes from the single charges decayed as approximately $R^{-2.4}$, and amplitudes from the row-charge decayed as $R^{-1.7}$. A dependence of amplitudes on depth of burst exists, and a yield scaling exponent near 0.8 appears to be appropriate.

It is suggested that a variation of particle velocity with distance as $R^{-A}e^{-kfR}$, where f is the signal frequency, is a more physically realistic description of attenuation than is the inverse power law. The preliminary data from the 140-ton row charge appear to fit this type of attenuation law, and indicate that A = 0.5 and k = 0.015 sec/km. An estimate is made of the near-source variation of peak seismic amplitude with frequency for the row charge, and predictions are made for possible future row-charge cratering experiments at the site.

Preface

This report is a summary of the essential features of the seismic investigations performed during the three phases of the Project Pre-Gondola high explosive cratering experiments which have been completed to date. One purpose of this report is to illustrate the continuity of the seismic measurements programs which are reported in detail by Power[1] and Ballard.[2] An attempt has been made to place the various data in their proper perspective with regard to the concept of seismic site calibration employed at the Fort Peck site.

The authors gratefully acknowledge the critical review and comment by Dean Power of the Lawrence Radiation Laboratory (LRL) and Robert Ballard, Jr., of the U. S. Army Engineer Waterways Experiment Station (WES), and their assistance in providing additional data. Russell Needham of the LASA Data Data Center in Billings, Montana, cooperated in providing the LASA recordings of the Pre-Gondola events.

Contents

TABLES

FIGURES

Figures (Continued)

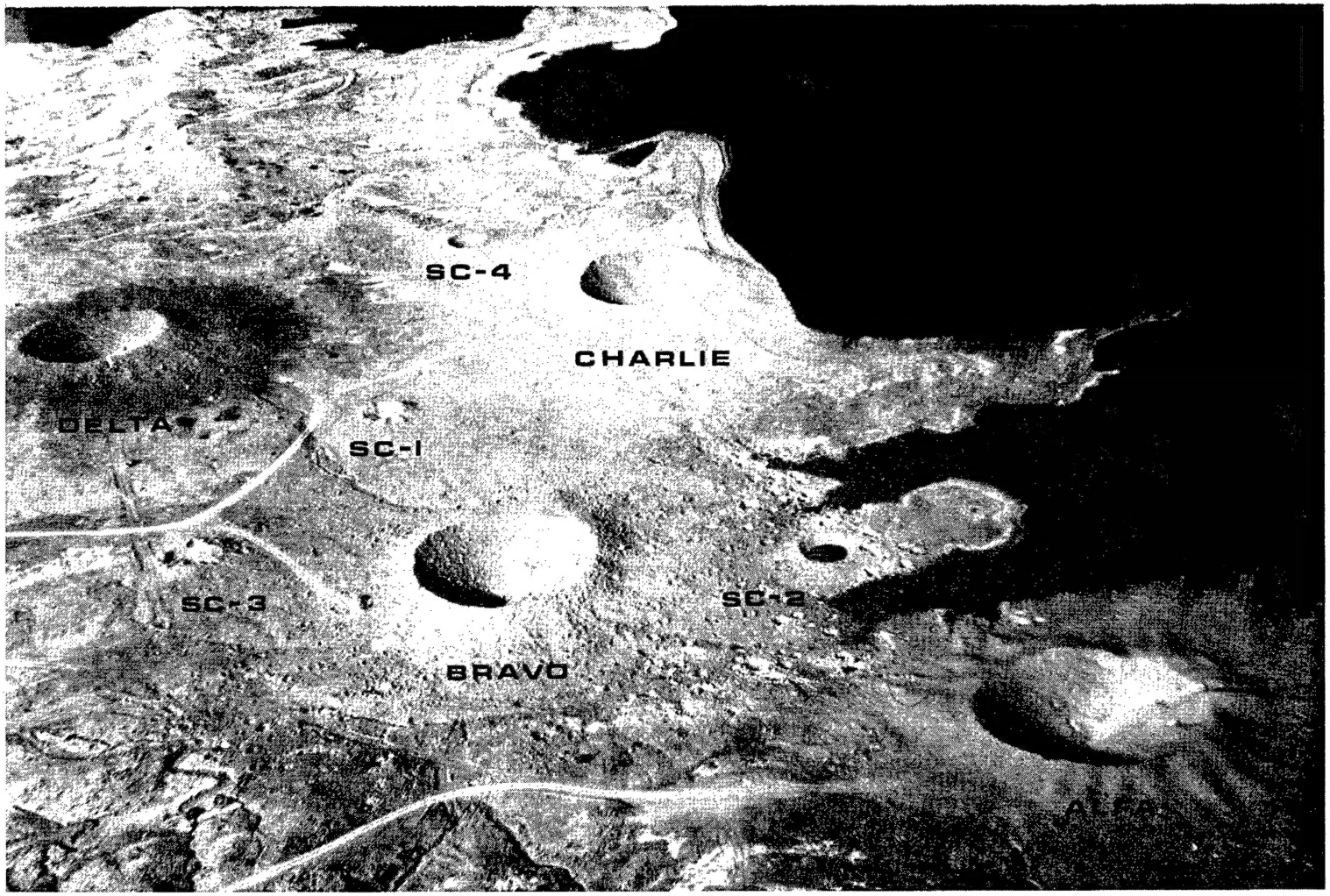

Frontispiece—Pre-Gondola craters, 4 November 1966.

Introduction

PURPOSE

The purpose of this report is to present the concepts, programs, and results of the seismic calibration activities at the Pre-Gondola high explosive (HE) cratering site at Fort Peck, Montana. It is believed that this documentation will be useful to those planning seismic site calibration experiments in other locations.

SCOPE

This report accounts for seismic measurements during the Pre-Gondola Seismic Site Calibration series, Pre-Gondola I, Pre-Gondola seismic decoupling experiments, and Pre-Gondola II. The Introduction describes the background, geology, technical objectives and programs, and the explosive charges. "Operations" covers the field operations and the instrumentation for the seismic measurements programs. Results are presented next, followed by an analysis of the results. Next appears the interpretation of the results as they relate to seismic calibration of the test site and predictions for Pre-Gondola III. Finally, the conclusions and recommendations are presented. Detailed results from the four series are tabulated in Appendix A.

BACKGROUND

Project Pre-Gondola is a series of chemical HE single- and row-charge cratering experiments in weak, wet clay-shale conducted by the U. S. Army Engineer Nuclear Cratering Group (NCG) as part of the joint Atomic Energy Commission-Corps of Engineers nuclear excavation research program. The Pre-Gondola detonations were executed in Valley County, near the edge of the Fort Peck Reservoir approximately 18 mi south of Glasgow, Montana (Fig. 1). Prior to approval for the Pre-Gondola II experiment, it was necessary to calibrate the site in order to provide reliable predictions of the seismic signal expected at the Fort Peck Dam.

Concept

The seismic measurements program in effect for all Pre-Gondola cratering explosions through June 1967 were designed as a continuing integrated effort to determine the specific propagation characteristics in the Fort Peck area and to develop improved techniques of operation and interpretation. Preliminary measurements prior to Pre-Gondola II were used to develop prediction schemes which were then tested during Pre-Gondola II. Analysis and interpretation of results of Pre-Gondola II would be the basis for predicting effects from Pre-Gondola III.

Seismic Site Calibration Series

The Pre-Gondola Seismic Site Calibration series (SSC) was designed to relieve concern for the safety of the Fort Peck Dam when subjected to ground motion from experiments at the 20-ton level and to provide a basis for developing a meaningful prediction for the effects of larger yield row-charge cratering experiments. The site had been selected after preliminary reconnaissance and geologic and engineering investigations indicated that the site met the overall project requirements and was

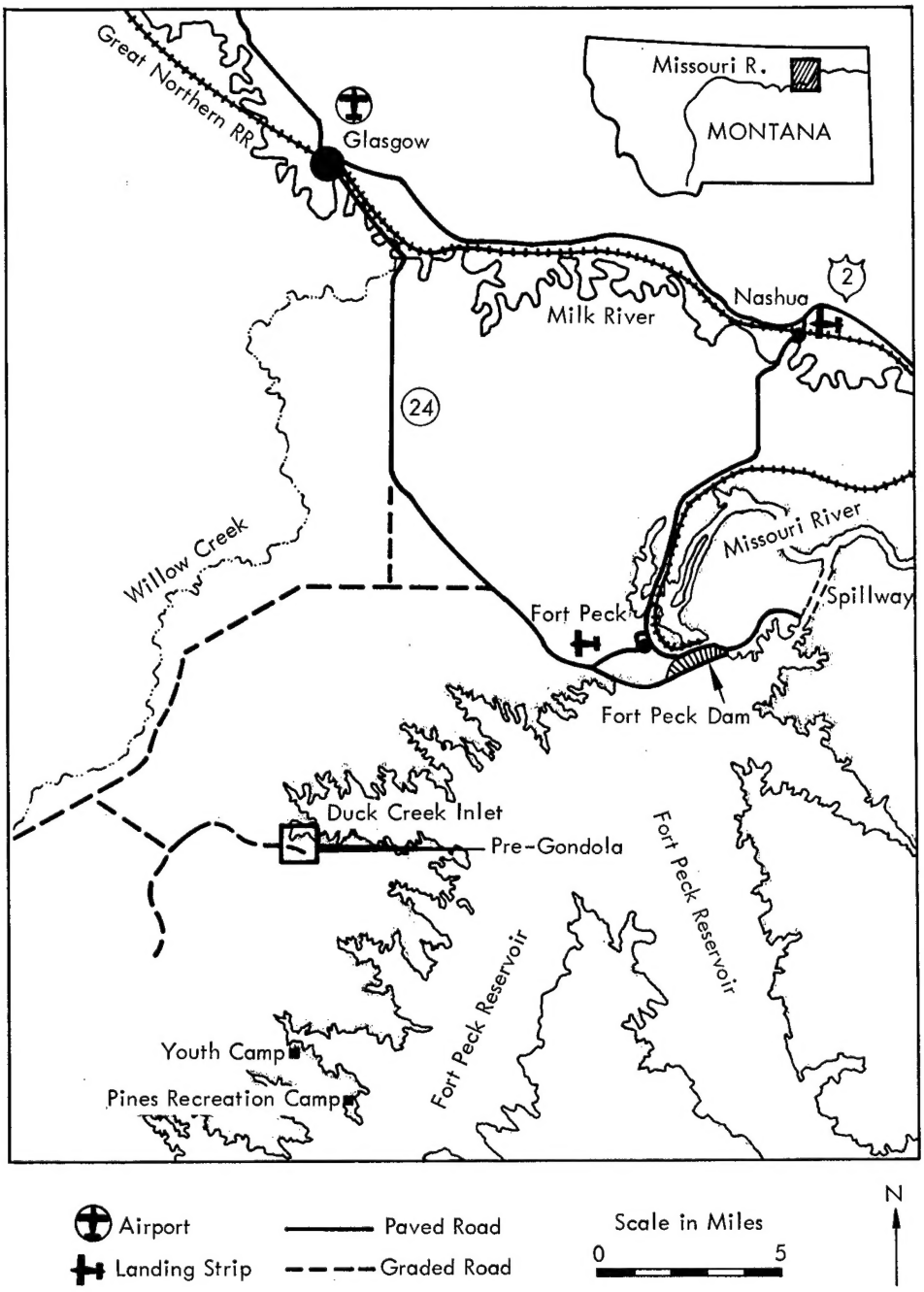

Fig. 1. Site map.

superior to others.[3] In order to obtain a preliminary safety and technical evaluation of seismic propagation in the region, four 1000-lb spherical charges of nitromethane were detonated at different depths of burst (DOB) in June 1966. The results assisted in seismic site calibration and provided preliminary cratering information for the design of the Pre-Gondola I experiment.

Pre-Gondola I

The purpose of Pre-Gondola I was to calibrate the project site with respect to its cratering characteristics and to provide a basis for the design of the proposed 140-

ton Pre-Gondola II and the Pre-Gondola III row-charge cratering detonations in the same medium.[4] Four 20-ton charges were detonated at various DOBs in October and November 1966. The results of both the SSC series and Pre-Gondola I were combined to produce a more refined seismic prediction scheme for the 140-ton Pre-Gondola II row-charge experiment. The appearance of the site at the completion of Pre-Gondola I is shown in the frontispiece.

Pre-Gondola Seismic Decoupling Experiment

The Pre-Gondola seismic decoupling experiment was designed to test the feasibility and effects of cratering with an explosive charge partially decoupled from the surrounding medium by an air gap around the charge. Previous investigations at the 1-lb yield level[5] indicated that the concept could have merit if it enhanced crater dimensions. The experiment included detonation of two 1000-lb charges, one fully coupled, and one decoupled by placing the charge sphere at the center of a cavity with a volume equivalent to 2000 lb of explosive. The charges were detonated at similar DOBs in mid-June 1967, prior to Pre-Gondola II. Seismic measurements were compared to the results of similar 1000-lb detonations during the SSC series.

Pre-Gondola II

Pre-Gondola II was a 140-ton row-charge cratering experiment detonated in June 1967.[6] The design of the row was based upon the cratering characteristics of the medium that were acquired from the previous experiments. The row consisted of two 40-ton charges and three 20-ton charges. The row-charge excavation connected to the Pre-Gondola I Charlie crater. Figure 2 shows the site layout for all detonations.

Pre-Gondola III

Pre-Gondola III is planned as a row-charge crater experiment connecting to the Pre-Gondola II crater along the same general alignment (Fig. 2). The experimental design and total yield will be established after analysis of all Pre-Gondola II results.

REGIONAL GEOLOGY AND LOCAL SITE CONDITIONS[3]

Regional Geologic Setting

Figure 3 shows the physical geography of the region around the Fort Peck site and the two alternate sites examined as possible locations for Pre-Gondola. The Fort Peck site is located a few miles south of the thick glacial drift of northeastern Montana. Thin glacial deposits occur in the area, but in most places they have been removed by erosion.

Stratigraphy. The northern Great Plains are underlain by a thick succession of nearly flat-lying marine and fresh-water strata of Cretaceous and Tertiary age. The deposits rest unconformably on older Mesozoic and Paleozoic rocks.

Figure 4 shows the general stratigraphy of the Fort Peck region and the stratigraphy of Project Pre-Gondola site medium (Bearpaw shale). The upper Cretaceous formations include thick layers of soft, compaction-type, marine shales. They are separated by coarser siltstones and sandstones and in some horizons by calcareous shales, limestones, and marls. The Bearpaw and Clagget shales, which

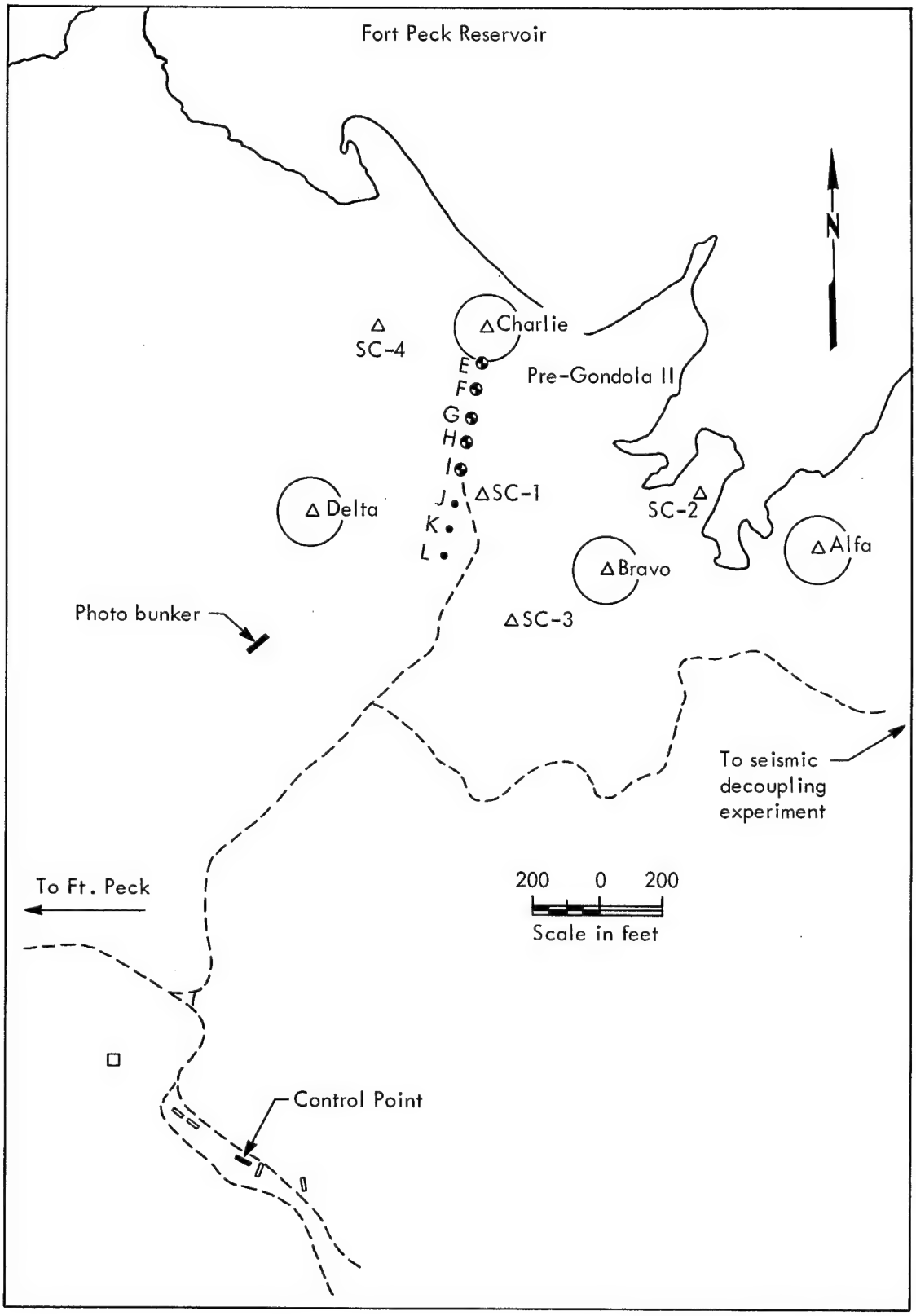

Fig. 2. Site layout.

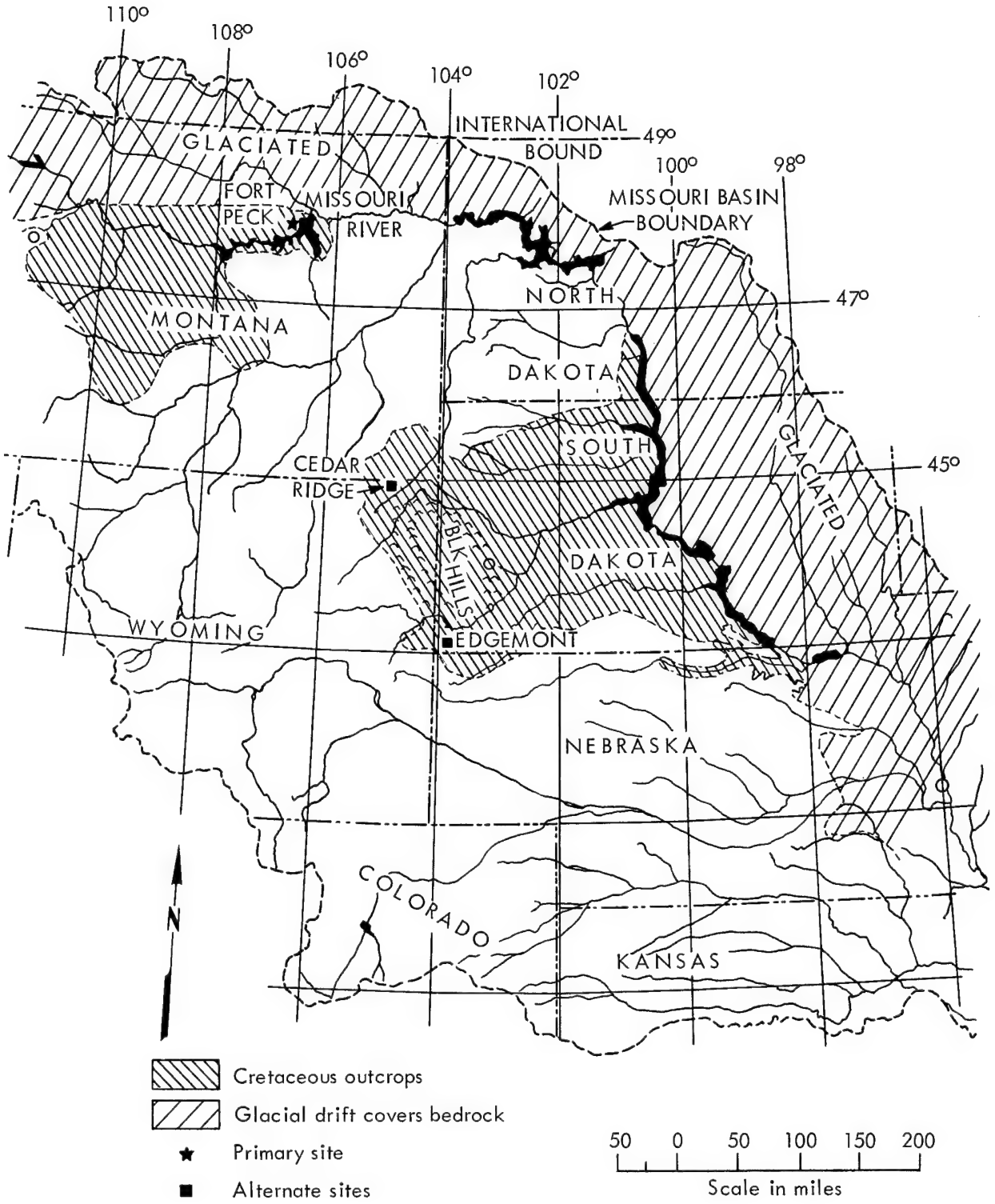

Fig. 3. Physical geography of region (Ref. 3).

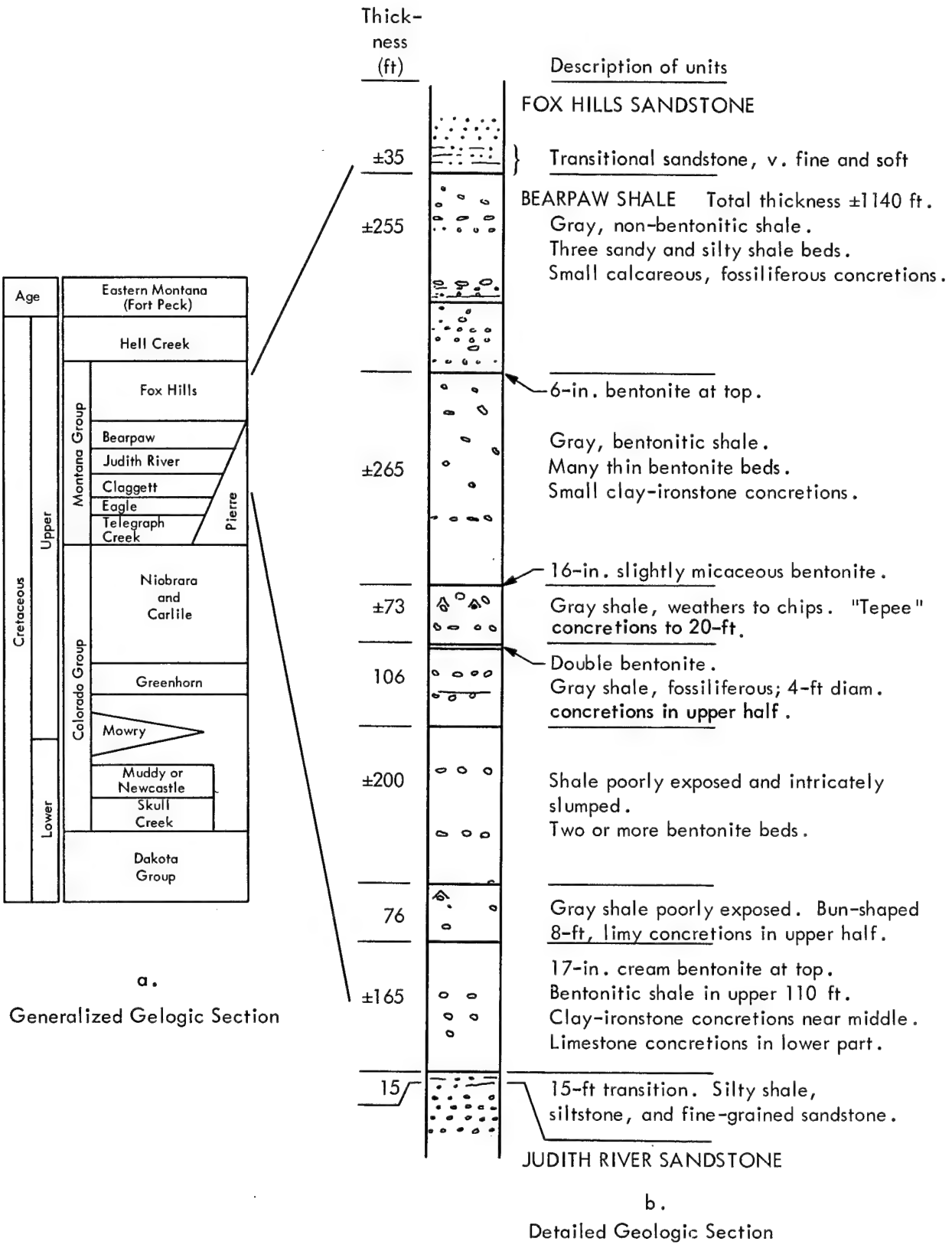

Fig. 4. Geologic sections, Fort Peck area (after Dudley—Ref. 3), a. generalized geologic section, b. detailed geologic section.

correlate with the upper member of the Pierre, are exposed in the Fort Peck Reservoir area.

Structure. The major bedrock structures of eastern Montana are broad and open, generally dipping only a few tens of feet per mile. The Pre-Gondola site, located at the edge of the Fort Peck Reservoir, is about 50 mi southeast of the Bowdoin dome, 60 mi north of the broad Blood Creek-Sheep Mountain anticline, and on the extreme western margin of the Williston basin. The Williston basin, centered in western North Dakota, is the largest geologic structure in this part of the Great Plains. In the vicinity of the Fort Peck site, the regional dip is southeast at about 25 ft/mi.

Site Conditions

Location and Land Use. The Pre-Gondola site is situated on the south fork of Duck Creek, adjacent to the Fort Peck Reservoir in Section 11, T25N, R39E, Valley County, Montana (Fig. 1). There are no inhabited dwellings within 4 mi of the site. The nearest population center is the town of Fort Peck, located 10 mi to the northeast. It has a population of about 650 people, mostly government employees engaged in the operation and maintenance of nearby Fort Peck Dam. The nearest structures are the huge earthfill embankment of the dam and the Fort Peck powerhouse, about 11 mi northeast of the site.

The primary reason for selecting a site at the edge of a reservoir was to take advantage of the expected high moisture content and possible water table at shallow depths. Because most of the shale at the site has been below reservoir level for many years, it was expected to be in a saturated or near-saturated condition.

Physiography. Where the Bearpaw shale outcrops, it forms either badlands or a terrain of small hills with moderately steep-to-gentle slopes and sparse vegetation. Drainage courses entering the Missouri trench from the north have eroded relatively short, steep-sided gullies forming the so-called "Missouri Breaks." The full difference in elevation between the Missouri floodplain and the ridges along the main reservoir is not apparent since the valley is inundated to a depth of nearly 250 ft by the reservoir. Along the Duck Creek inlet, however, the land adjacent to the reservoir is primarily gently rolling terrain situated slightly above reservoir level. There are a few narrow ridges with moderately steep sides, providing a variety of topographic conditions.

Stratigraphy. The Bearpaw shale of late Cretaceous age forms the bedrock at the Pre-Gondola site and outcrops over most of the area. It is underlain at a depth of approximately 900 ft by the Judith River formation, a mid-Upper Cretaceous sandstone. The uppermost few hundred feet of the Bearpaw shale and the overlying Fox Hills sandstone, which caps the higher ridges along the reservoir south of the Pre-Gondola site, have been removed by erosion. An additional but unknown thickness of Tertiary and younger sediments, once overlying the area, have also been eroded. Thin scattered remnants of glacial deposits indicated that Pleistocene glaciers advanced over the site.

The shale at the Pre-Gondola site is uniform, dark gray, highly compacted, and

uncemented. It contains infrequent calcareous and iron-manganese concretions up to 1 ft thick, and waxy, light gray-to-tan bentonite layers. Several joint sets with inconsistent orientation occur at spacings of 1/2 to 3 ft, and numerous hairline cracks are visible between the major joints.

The base of the weathered zone occurs at depths of 10 to 20 ft. The visible effects of weathering include increased fracture frequency, opening of joints, and oxidation and mineral filling along joints and fractures. Within a few feet of the surface the shale is highly fragmented. Alternate wetting and drying at the surface causes further breakdown of the shale particles to form a fat clay. There were variations in the detailed geology between the specific sites for charge emplacement. At the Bravo site, the shale was covered by a mantle of 5 to 6 ft of glacial till and alluvium, and at the Delta site the shale was covered by an insignificant amount of overburden. Weathering effects were observed to depths of about 5 ft at the Alfa and Bravo sites, while at the Charlie and Delta sites the effects of weathering extended to depths of about 14 ft.

Ground Water. Because it is highly compacted and contains montmorillonite (a clay mineral with the ability to attract and hold water by electrical bonding), the unbroken and unweathered shale is essentially impervious, and any appreciable movement of water occurs only through fault or fracture zones. Static water levels in observation wells open in the weathered shale show that the water table at the Alfa and Bravo sites is about 6 ft beneath the ground surface, while at Charlie and Delta it is about 15 ft. A Casagrande piezometer with the sand tip in unweathered shale at the Charlie site stabilized at a depth of 75 ft. This indicates that movement of water occurs primarily along fractures and that independent ground-water systems may occur within different fracture systems in the shale. In the lowlands adjacent to the reservoir, the more pervious overburden and weathered shale extend to depths well below the reservoir level, and the water table is adjusted to the pool.

Engineering Properties of Site Medium

The range of the physical properties of the Bearpaw shale at the Pre-Gondola site is shown in Fig. 5.

Strength. The laboratory unconfined compressive strength of the intact shale is high; however, the mass strength of the in situ material is reduced by the bentonite seams and an extensive system of jointing and slumping. Figure 5 shows the general increase in strength with depth. The range

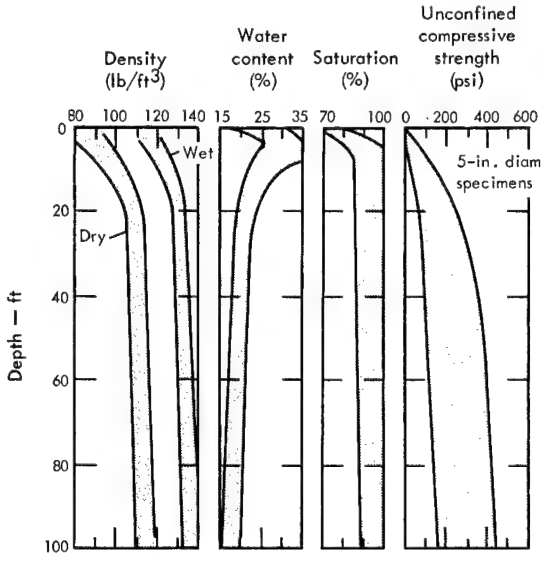

Fig. 5. Range of physical properties of Bearpaw shale, Pre-Gondola site.

of strengths probably reflects differences in fracturing rather than in the strength of the intact shale. Undrained triaxial compression tests on small-diameter, intact samples from the Bravo and Charlie ground-zero boring confirm that the strength does increase with depth.[4]

Moisture. Water contents range from as much as 30% near the surface to a rather consistent 16 to 18% at depth. Although most of the samples recovered were 100% saturated, a few were as low as 75%. The porosity ranges from 25 to 52%, and averages about 32%.

Density. The unweathered shale at the Fort Peck site has an average in situ wet density of 134 lb/ft^3 and a dry density of approximately 112 lb/ft^3. Samples recovered from the weathered zone are less dense and quite variable, with wet bulk densities of 110 to 125 lb/ft^3 and dry densities of 90 to 105 lb/ft^3 (Ref. 3).

Classification. When the shale is remolded, it classifies as a fat clay (CH), with a plastic limit of about 26% and a liquid limit ranging from 60 to 200%.

Seismic Velocity. The average seismic velocity for unweathered Bearpaw shale at the Pre-Gondola site (to a depth of approximately 100 ft) is 6800 ft/sec.

TECHNICAL OBJECTIVES

The specific technical objectives listed below were established to accomplish a reliable seismic calibration of the test area by empirical means.

Source Mechanism

1. To evaluate the effect of variation in DOB on the amount of seismic energy coupled into the ground.
2. To acquire an evaluation of the yield-scaling assumptions.
3. To determine the effect of a distributed row charge compared to a single cratering charge where individual charge weights are comparable.

Transmission Characteristics of Region

1. To investigate the propagation characteristics of the region surrounding the Fort Peck area.
2. To investigate the transmission of seismic energy through the Fort Peck Reservoir.
3. To determine the presence of any directional asymmetry of propagation.

Receiving Station

1. To document the response of certain major structures in the vicinity of Fort Peck.
2. To provide measurements for use in a separate LRL-sponsored analytical study of the response of earth embankments to seismic loading.

TECHNICAL PROGRAMS

Individual Programs

In order to meet the objectives outlined above, three main technical programs were established for the Pre-Gondola SSC, Pre-Gondola I, and Pre-Gondola II events and implemented to a limited extent during the seismic decoupling experiment.

Intermediate Range Measurements. This program to study seismic propagation

involved the measurement of ground motion amplitudes at a number of locations along radial lines extending out to intermediate* distances from surface ground zero (SGZ). The program was conducted by LRL.[1]

Structures Instrumentation. This program consisted of the documentation of seismically induced motion at the Fort Peck Dam and other major structures associated with the dam. The U. S. Army Engineer Waterways Experiment Station (WES) operated the recording stations for this study of structural response.[2]

Earth Dam Response. The measurement and analysis of the dynamic response of the embankment portion of the Fort Peck Dam was the responsibility of Montana State University (MSU) under the sponsorship of LRL. The purpose of this program is to develop a general understanding of how earth fill embankments respond to seismic loading. Formal results of this program are not available at this time.

*The meaning of "intermediate" range is not well defined. The boundaries which separate "close" range from intermediate range, and intermediate range from "teleseismic" range have not been defined in absolute quantitative terms. A distinction in these regions can be made according to the instrumentation commonly used to record the seismic motions. Measurements at close ranges are generally made with accelerometers because this type of transducer is suitable for the large ground motion amplitudes characteristic of this region. Velocity transducers are commonly used to record intermediate range motions. These transducers are suitable for the range of motions from near damage thresholds to well below the threshold of human perception. Displacement recorders are most suitable for teleseismic distances because of their high sensitivity and good low-frequency response, as manifested in the typical observatory seismograph.

Yield Escalation

Progressively higher yields were used for seismic calibration in order to assure greater confidence in prediction. The 1000-lb SSC series furnished preliminary information concerning peak seismic amplitudes, their attenuation with distance, and the effect of DOB on seismic coupling. This preliminary information was used to estimate both the maximum ground motions and the structural response for the subsequent 20-ton Pre-Gondola I series. Based on these estimates, the seismic recorders were adjusted to appropriate gain levels for the 20-ton events to insure maximum data recovery.

The gain levels for recorders used during the 140-ton Pre-Gondola II Event were set after an analysis of Pre-Gondola I results and formulation of prediction procedures.[1,2,6] The seismic decoupling experiment also provided an opportunity to calibrate new seismic instrumentation stations for Pre-Gondola II[5] at stations not in existence for Pre-Gondola I.

Analysis and interpretation of the Pre-Gondola II results[7] provide prediction equations for future experiments at the site.

Validation of Decoupling Concept

In addition to satisfying the seismic site calibration objectives, the technical programs also allowed a comparison of the seismic effects for coupled and decoupled charges during the seismic decoupling experiment. Earlier results of seven NCG laboratory scale tests were interpreted as indicating that 1-lb decoupled charges produced larger craters than charges of similar yield and DOB that had not been

decoupled from the medium.[5] This relationship appeared to exist even when the decoupled charges were buried so that the top of the decoupling void was at the same depth as the top of the coupled charges. The 1000-lb seismic decoupling experiment was intended to validate these preliminary data at a significantly higher yield level in a well-calibrated medium.

DESCRIPTION OF HIGH EXPLOSIVE CHARGES

The following paragraphs describe the details of the HE charges used as seismic sources. The explosive used was liquid nitromethane (CH_3NO_2) which was center-detonated with a booster charge of C-4 explosive. Fill and vent lines were sand stemmed.

Seismic Site Calibration Series

Figure 6 shows the aluminum container used for the 1000-lb charges with booster, fill, and vent lines attached. The 42-in. diam emplacement hole (Fig. 7) was stemmed with a lean mix concrete plug placed after the container was in position (Fig. 8). Sand stemming was placed by dumping and hand tamping.

Pre-Gondola I Series

Figure 9 shows the design of the explosive charge emplacement for the 40,000-lb (20-ton) charges. A mined spherical cavity was constructed at the bottom of a 38-in. diam emplacement hole. The access hole stem design (grout) was designed by WES to react to the cratering mechanisms of the explosion in the same manner as the surrounding in situ material.[4] The stem

Fig. 6. Charge (1000-lb) for seismic site calibration series and coupled shot of seismic decoupling experiment.

configuration provided a total shear resistance equal to the total unconfined dynamic shear resistance of the in situ shale mass developed by bond (concrete to clay-shale).

Seismic Decoupling Series

The decoupled charge (Fig. 10) consisted of a SSC-type 1000-lb aluminum explosive container centered in a sheet metal sphere which provided a 4-3/4 in. air space between the explosive and the surrounding shale. The volume of the air space was equal to that of the 1000-lb coupled charge sphere. Both charges were emplaced in 48-in. diam holes which were completely stemmed with grout (Fig. 11).

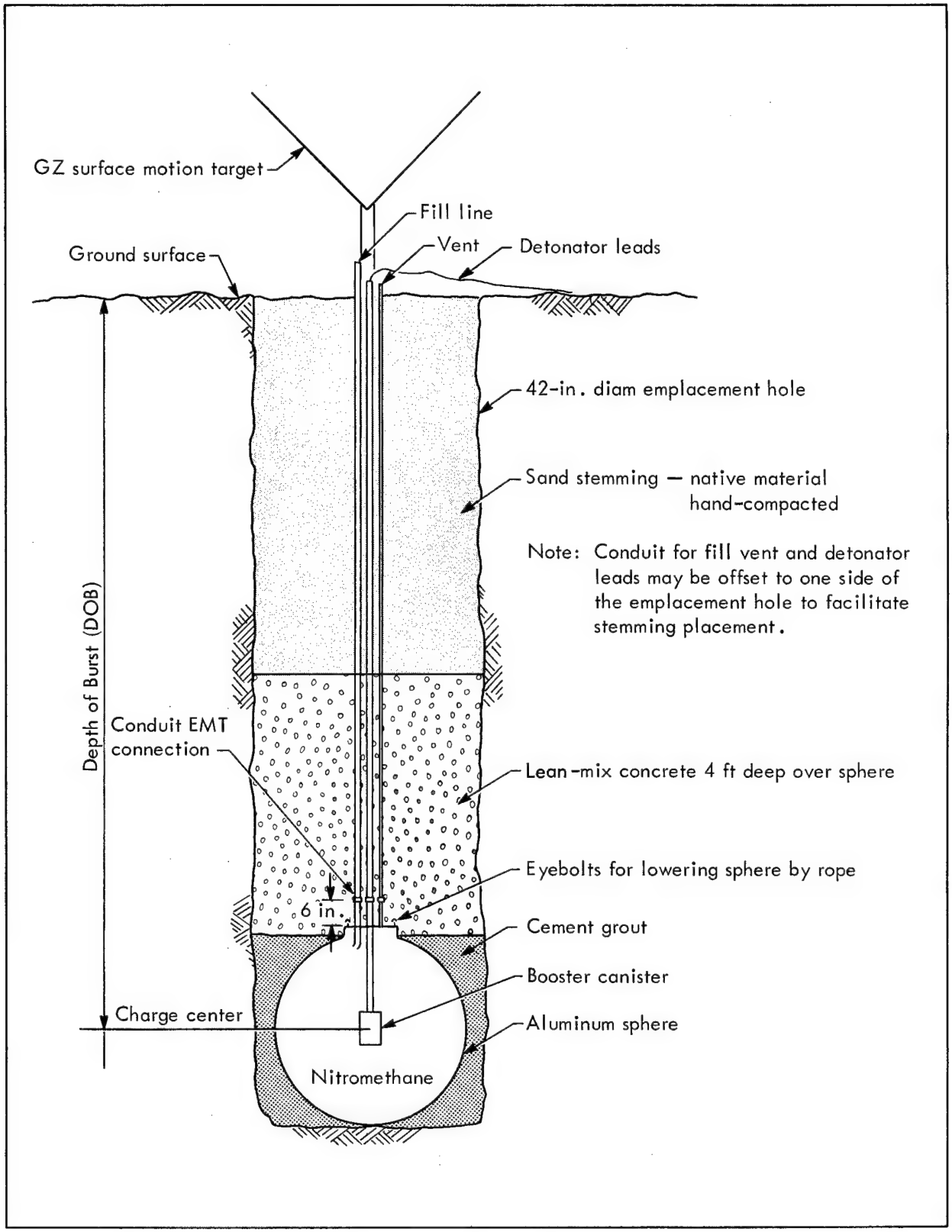

Fig. 7. Charge emplacement for Pre-Gondola seismic experiment.

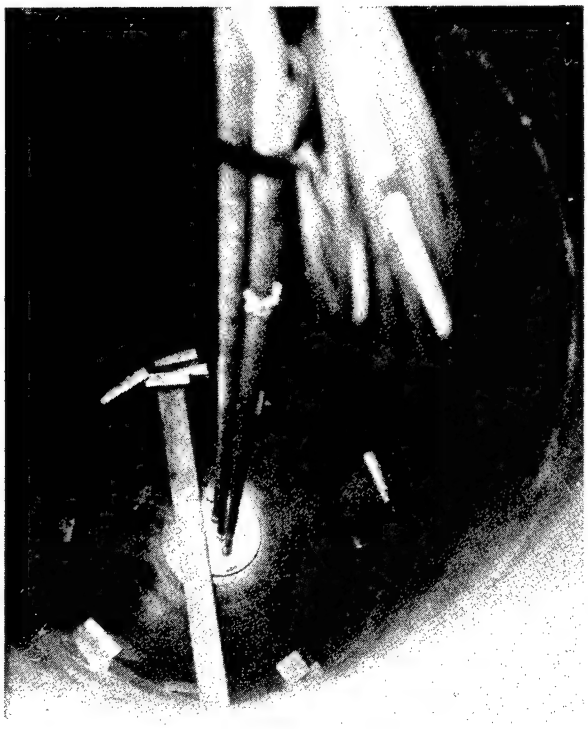

Fig. 8. Emplaced 1000-lb charge prior to grouting.

Pre-Gondola II

Three 20-ton and two 40-ton charges, similar to those used during Pre-Gondola I, were used for Pre-Gondola II (Fig. 12). The five charges in a row (Fig. 2) were detonated simultaneously.

DESCRIPTION OF DETONATIONS

Table I lists the time and place of detonation for each event of each series described in this report.

Table II lists the charge weight, depth of burst, and resulting apparent crater dimensions for each event.

Table I. Detonation schedule

Event	Date	Time (MST)	Longitude	Latitude
1000-lb Seismic Site Calibration Series				
SC-1	20 Jun 66	0845	W 106° 38' 30.573"	N 47° 55' 48.383"
SC-4	21 Jun 66	0811	W 106° 38' 35.059"	N 47° 55' 53.380"
SC-2	22 Jun 66	0805	W 106° 38' 20.792"	N 47° 55' 48.181"
SC-3	23 Jun 66	0837	W 106° 38' 29.495"	N 47° 55' 44.579"
40,000-lb Pre-Gondola I Series				
Bravo	25 Oct 66	1000:00.760	W 106° 38' 24.894"	N 47° 55' 46.154"
Charlie	28 Oct 66	1200:00.654	W 106° 38' 29.974"	N 47° 55' 53.294"
Alfa	1 Nov 66	1000:00.275	W 106° 38' 15.325"	N 47° 55' 46.570"
Delta	4 Nov 66	1000:00.032	W 106° 38' 38.134"	N 47° 55' 48.077"
1000-lb Seismic Decoupling Experiment				
SD-1 (coupled)	14 Jun 67	1745:00	W 106° 37' 57"	N 47° 55' 33"
SD-2 (decoupled)	14 Jun 67	1430:00	W 106° 37' 56"	N 47° 55' 36"
140-ton Pre-Gondola II Experiment				
Row charge	28 Jun 67	0800:00.000	W 106° 38' 31"	N 47° 55' 51"

Table II. Charge emplacement and crater dimensions

Event	Charge weight (tons NM)[a]	Depth of burst (ft)	Spacing (ft)	Apparent crater radius (ft)	Apparent crater depth (ft)
Seismic Site Calibration Series					
SC-4	0.5	12.2	-	24.5	13.0
SC-2	0.5	15.8	-	27.3	12.5
SC-1	0.5	19.1	-	7.1[b]	2.8[b]
SC-3	0.5	23.3	-	14.6[b]	3.4[b]
Pre-Gondola I Series					
Charlie	19.62	42.49	-	80.4	32.6
Bravo	19.36	46.25	-	78.5	29.5
Alfa	20.35	52.71	-	76.1	32.1
Delta	20.24	56.87	-	65.1	25.2
Seismic Decoupling Series					
SD-1 (coupled)	0.5	17.3	-	25.1	10.5
SD-2 (decoupled)	0.5	17.7	-	23.7	10.5
Pre-Gondola II Experiment					
Charge[c]				Apparent crater width	
Charlie (existing crater)					
E	38.61	59.7	105.5[d]	206.5	55.5
F	19.70	49.4	79.8[d]	152.5	37.5
G	19.55	48.8	79.9[d]	164.0	36.9
H	39.56	59.9	79.9[d]	214.5	57.0
I	20.00	48.8	79.9[d]	173.0	33.5

[a]Energy equivalent yield = tons NM × 1.1.

[b]Anomalous and very asymmetrical; may have produced a mound in level terrain.

[c]Row centerline oriented S11° W from center of Charlie.

[d]Distance from charge on line above.

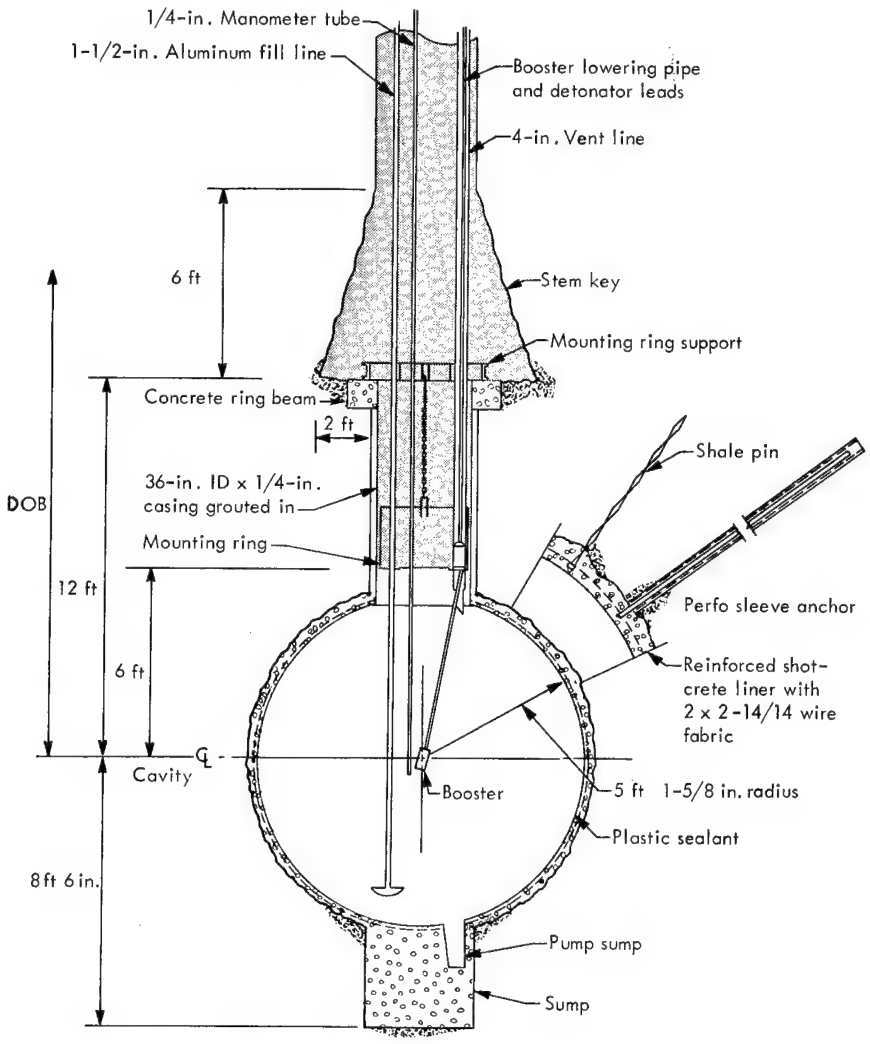

Fig. 9. Cross section of chemical explosive charge, Pre-Gondola I.

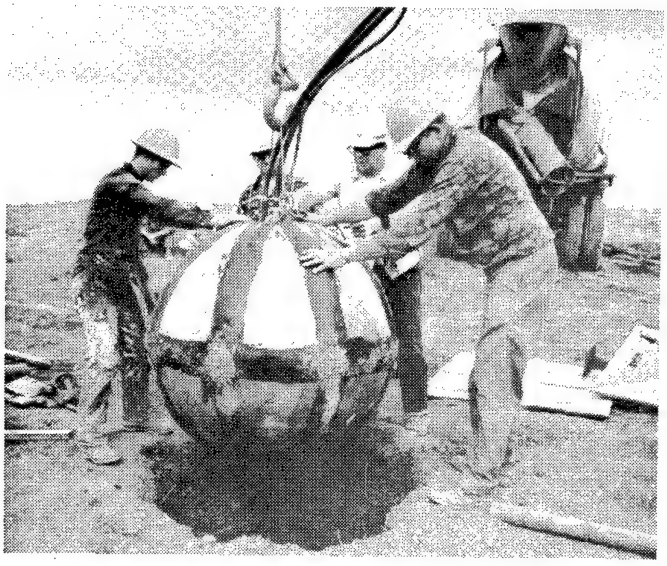

Fig. 10. Decoupled charge (1000-lb) being emplaced.

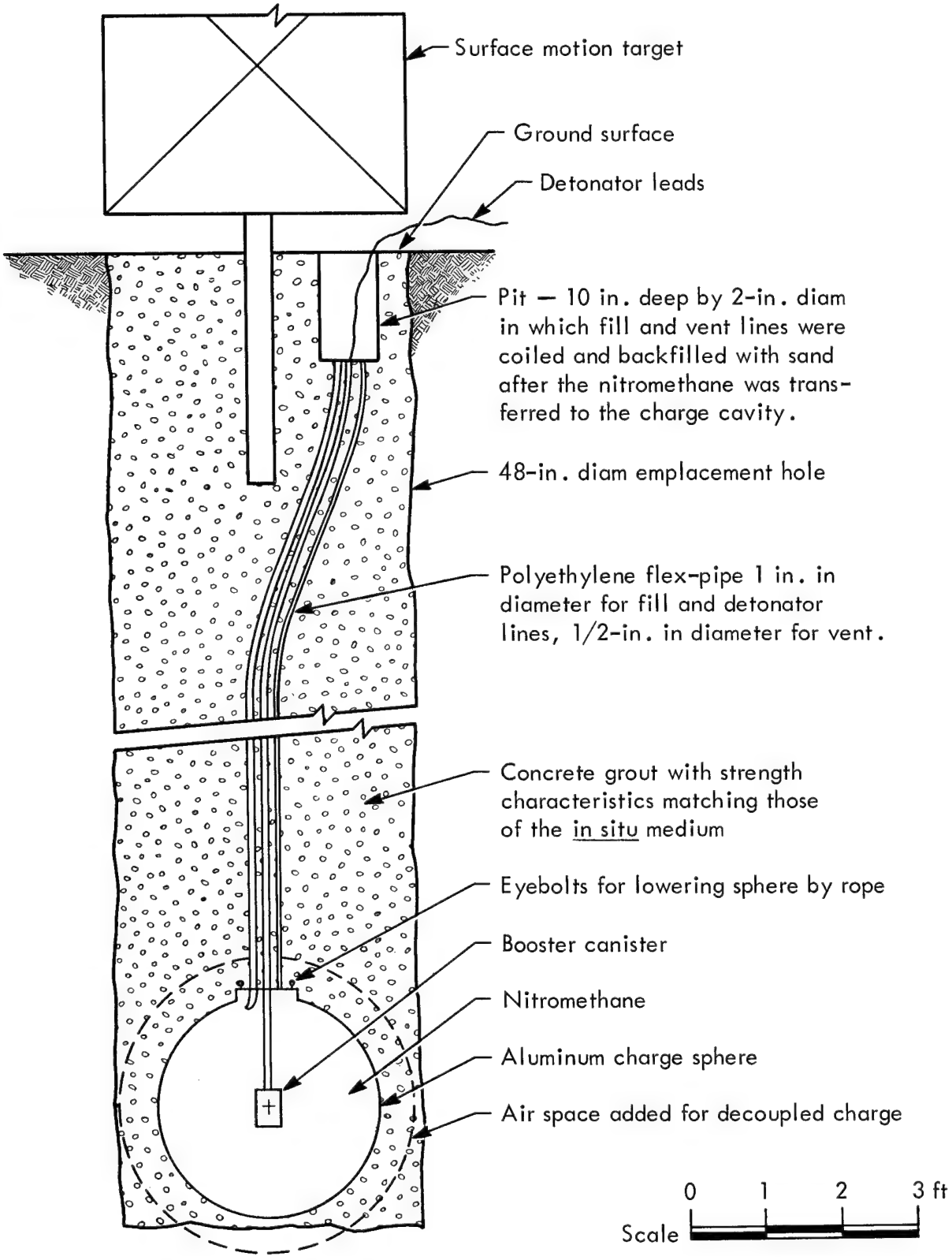

Fig. 11. Emplacement of 1000-lb nitromethane charge sphere for seismic decoupling series.

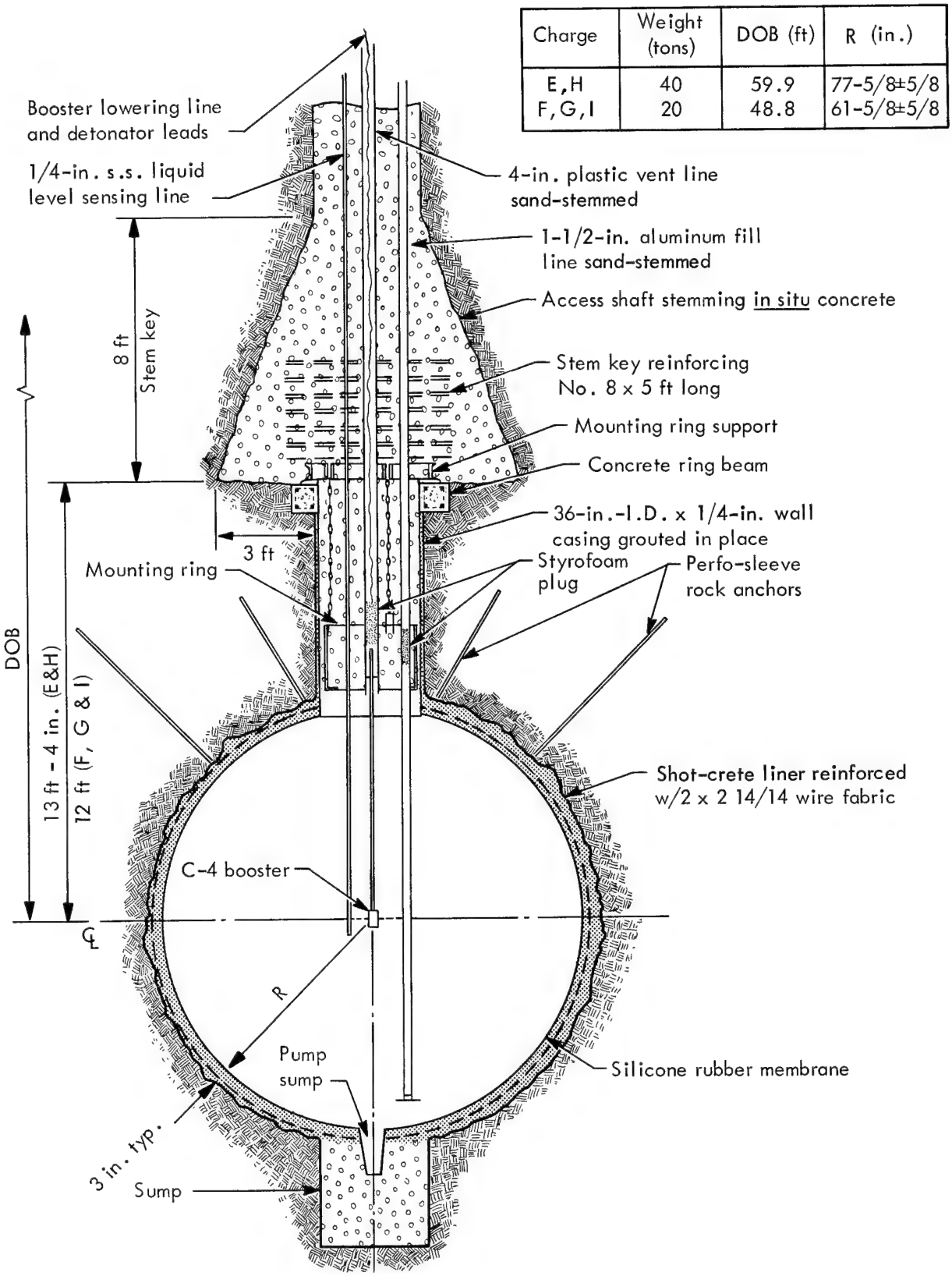

Fig. 12. Cross section of chemical explosive charge, Pre-Gondola II.

Operations

PROCEDURES

The field operations of the different agencies were quite similar and differed only in detail. Ballard[2] and Power[1] give complete discussions of techniques and of station operation. Procedures were modified slightly from event to event and from series to series. Communication between the seismic recording stations and Pre-Gondola Control through SSB and FM radio nets provided a means of coordinating the operations of the various seismic technical programs.

STATION LOCATIONS

Intermediate Range Stations

The intermediate range stations (Fig. 13) were spaced at logarithmically increasing intervals away from SGZ. Pertinent information about the station locations is tabulated in Table III.

The LRL instruments were located at the intermediate range stations for only one of the four events in the 1000-lb and 20-ton series, with the exception of one station which was left in place for the purpose of comparison. The instruments were moved to the dam for the remainder of the four events in each series to provide data for MSU.

Structures Instrumentation Stations

The WES structures instrumentation stations are shown in Fig. 14 and pertinent details are tabulated in Table III. Figure 15 is an aerial view of the Fort Peck Dam showing the locations of WES stations 1, 2, and 5. Figure 16 is an aerial view of the spillway and shows the locations of WES stations 3 and 4.

WES stations 4 and 5 were established and monitored for the seismic decoupling experiment and Pre-Gondola II only. In addition, a hydrophone was placed in the reservoir several hundred feet out from the face of the dam during Pre-Gondola II.

INSTRUMENTATION

Both the LRL and the WES instrumentation systems employed the same type of moving coil velocity transducers with a nominal natural frequency of 1 Hz. Detectors were arranged in triaxial arrays with the horizontal components oriented radially and transversely to SGZ.

For Pre-Gondola I and II, all LRL velocity transducers were mounted in rigid triaxial frames (Fig. 17) which in turn were housed in protective fiberglas canisters. These geophone assemblies were buried 12 to 18 in. below the ground surface at each station. Figure 18 shows such an assembly being lowered into an augered hole. The canister was oriented, levelled, and firmly emplaced by tamping sand around it. A complete LRL station is shown in Fig. 19.

The output from the geophones and a timing reference signal were recorded on a four-channel FM tape system developed by LRL and illustrated in Fig. 20. Pen recorders were used at some of the intermediate range stations during the 1000-lb series.

At the WES installations, the transducers were individually attached to the

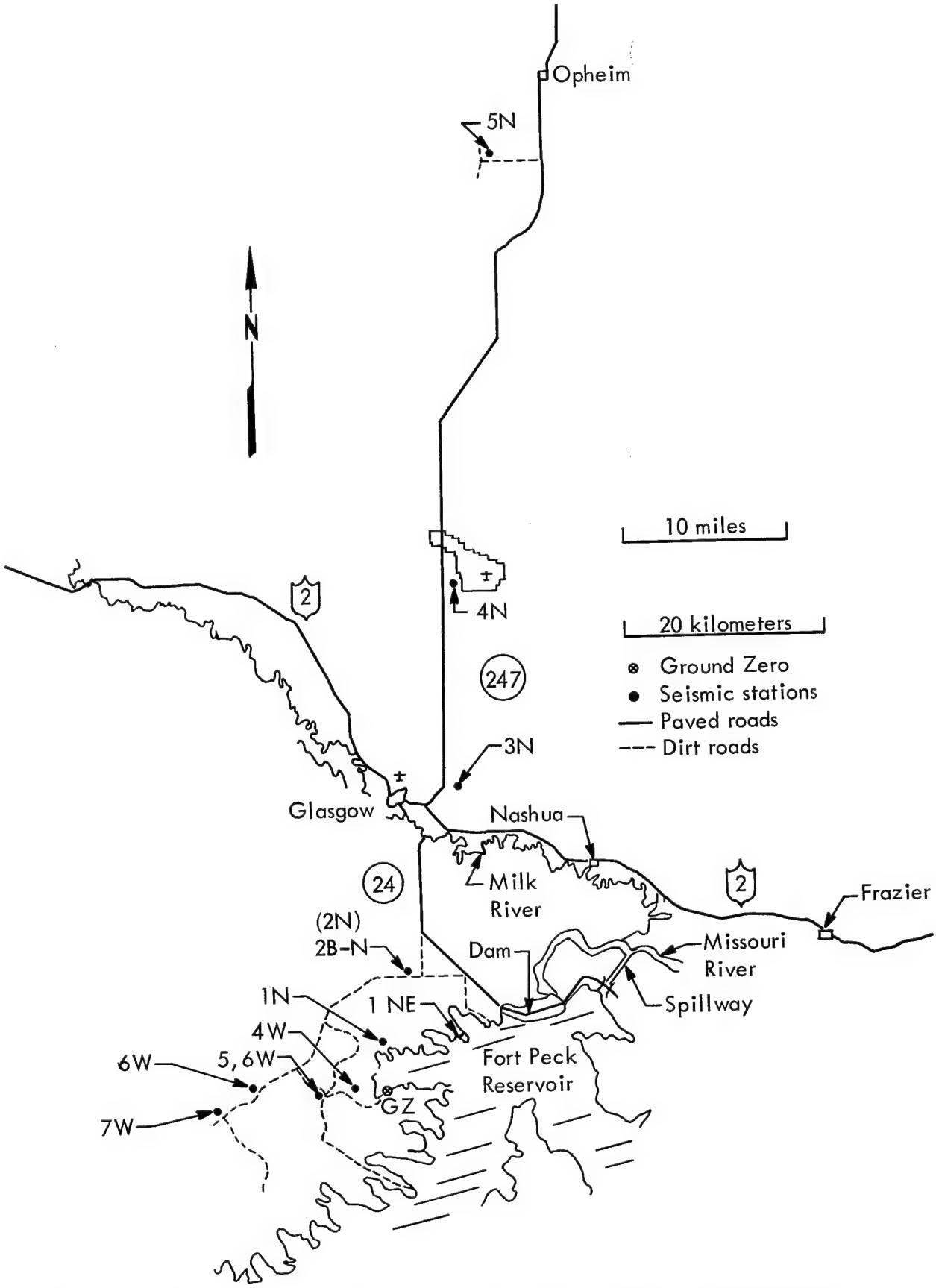

Fig. 13. Map showing locations of LRL intermediate range stations.

Table III. Locations of seismic recording stations.[a]

Series	Event	Station	Distance	Location
		LRL Intermediate Range Stations		
Seismic	SC-3	4W	3.2	W of SGZ
Site	SC-3	5W	6.2	W of SGZ
Calibration	SC-3	6W	13.8	W of SGZ
	SC-3	7W	20.7	W of SGZ
Pre-Gondola I	Bravo	1NE	8.75	NE of SGZ
	All	2N	11.65	N of SGZ
	Bravo	3N	29.3	N of SGZ
	Bravo	4N	52.0	N of SGZ
	Bravo	5N	95.9	N of SGZ
	Bravo	6W[b]	6.4	W of SGZ
		WES Structures Instrumentation Stations		
All	All	1	18.5	Top of dam at 58+00
	All	2	20.1	Gate control structure No. 3
	All	3	24.9	East wall of spillway
		4[c]	24.8	West bank of spillway
		5[c]	20.0	Top of power house No. 2

[a]The intermediate range stations for Pre-Gondola II were the same as for Bravo, with the exception of station 1NE, which was moved to a position 5.5 km due north of SGZ, and was then designated station 1N. Only LRL stations 2N and 6W were operated during the seismic decoupling experiment.

[b]Station 6W, Pre-Gondola I, is the same location as station 5W, SSC series.

[c]Stations 4 and 5 were added to the structures instrumentation program for Pre-Gondola II and the seismic decoupling experiment.

structure rather than mounted in a frame. Figure 21 shows three orthogonal geophones as installed at WES station 1 and at the LRL stations during the 1000-lb series. Figures 22 and 23 illustrate the installations at WES stations 2 and 3 respectively. The seismic signals were recorded on FM tape and on oscillographs at all of the WES locations.

The velocity transducers that were used are considered reliable and rugged enough for field applications. They are compatible with standard recording techniques, and possess a high sensitivity and flat response over the frequency range of interest.

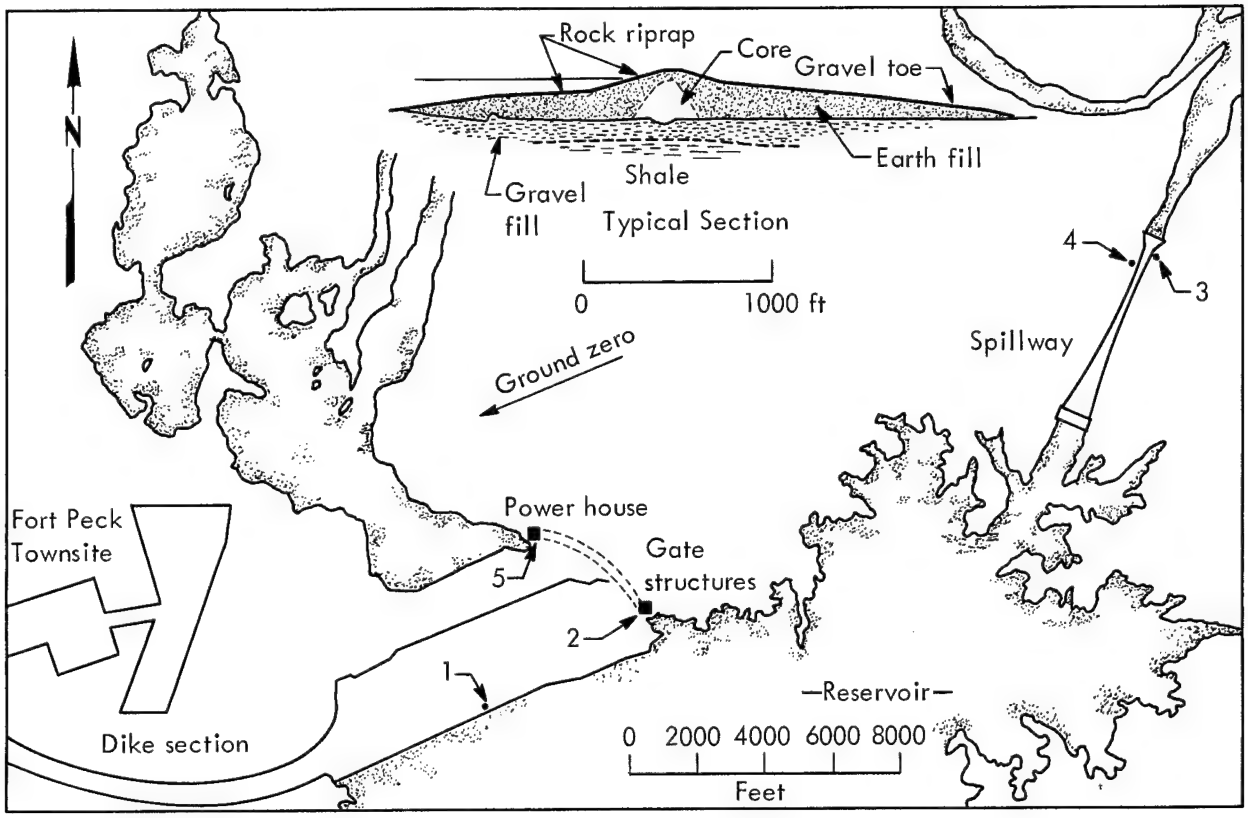

Fig. 14. Map showing locations of WES structures instrumentation stations.

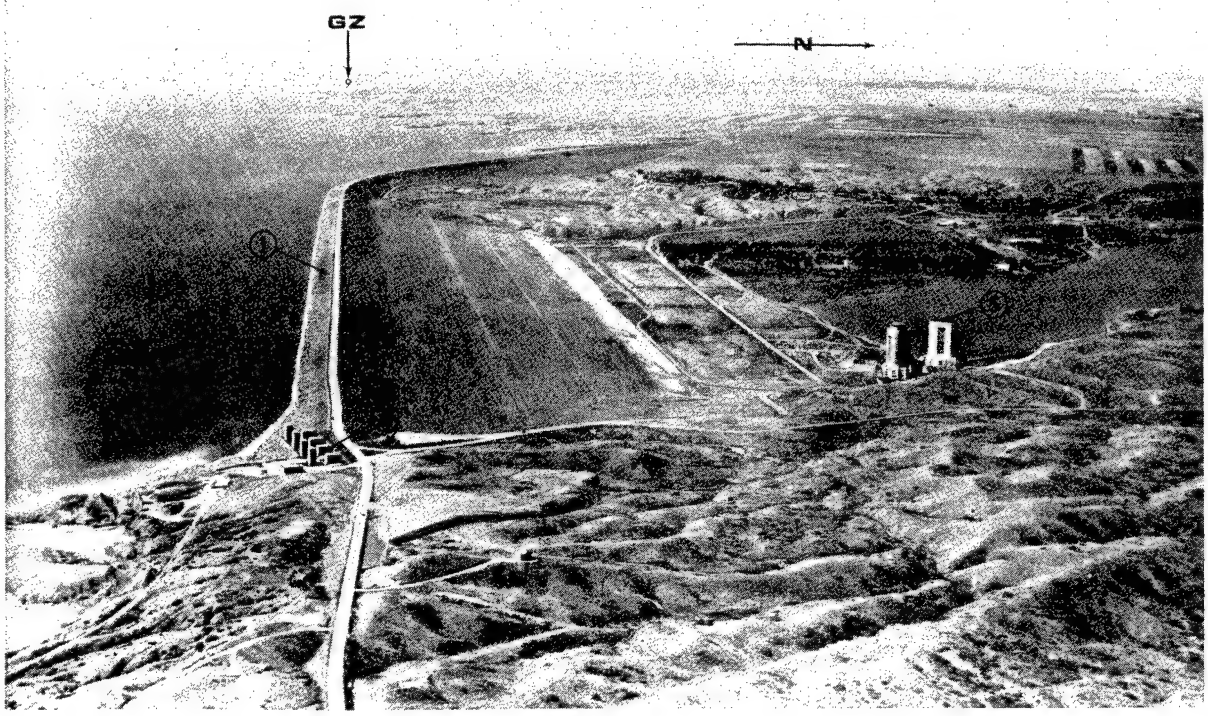

Fig. 15. Aerial view of Fort Peck Dam showing locations of WES structures instrumentation stations 1, 2, and 5.

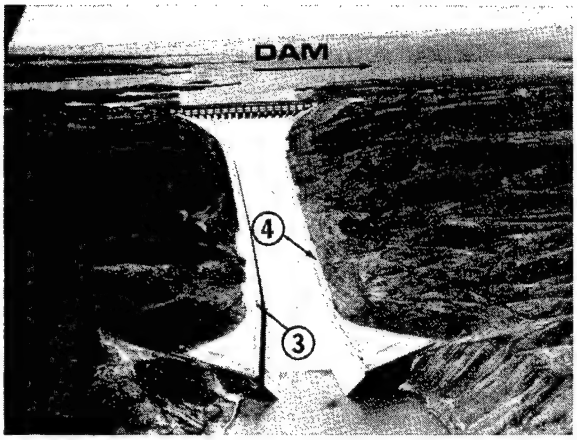

Fig. 16. Aerial view of spillway showing locations of WES structures instrumentation stations 3 and 4.

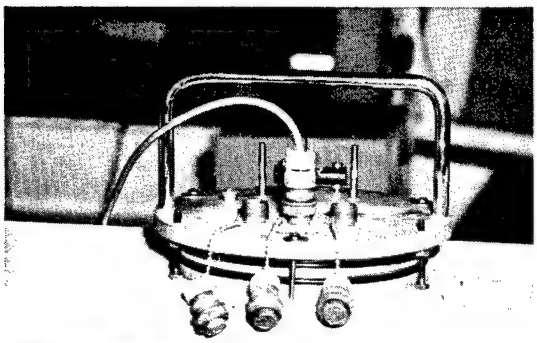

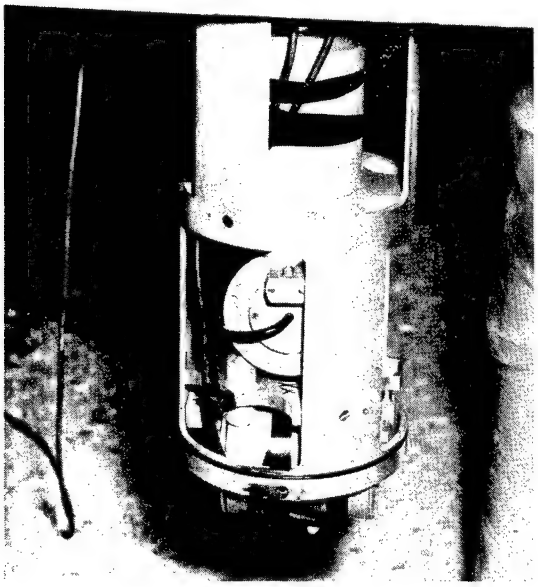

Fig. 17. LRL triaxial mounting frame for velocity detectors.

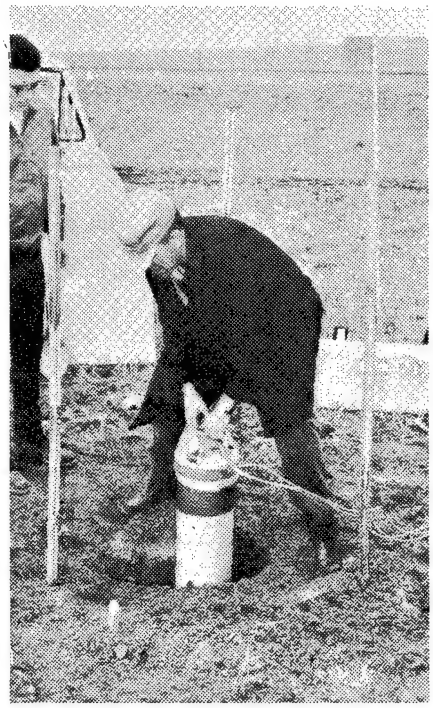

Fig. 18. Geophone assembly in fiberglas canister being placed in augered hole at LRL station.

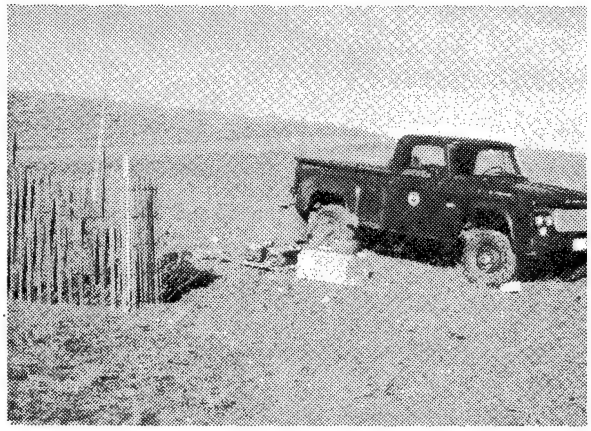

Fig. 19. LRL intermediate range recording station.

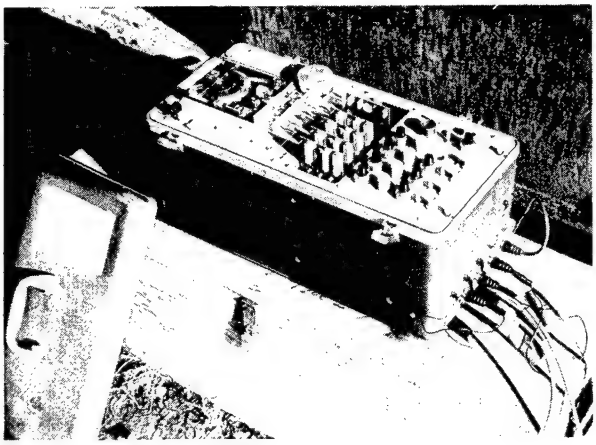

Fig. 20. LRL four-channel FM magnetic tape recorder.

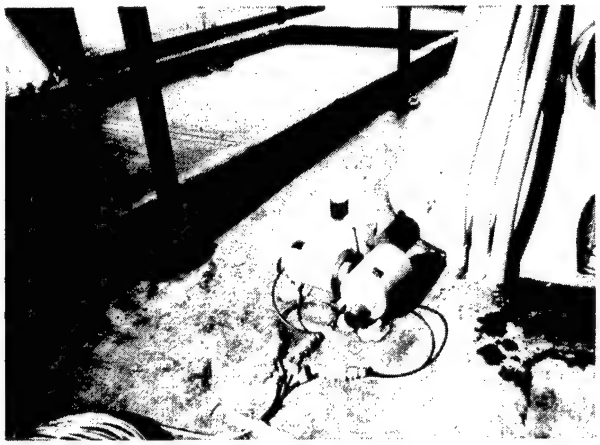

Fig. 22. Triaxial geophone array at WES station 2.

Fig. 21. Triaxial geophone array at WES station 1.

Fig. 23. Triaxial geophone array at WES station 3.

Results

This section presents the final results of the seismic technical programs for the SSC series, Pre-Gondola I, and the seismic decoupling experiments. The next section presents an analysis of the results contained in this section, predictions for Pre-Gondola II, and the preliminary results for Pre-Gondola II.

INTERMEDIATE RANGE MEASUREMENTS

The results of the intermediate range measurements program for the Seismic Site Calibration series and for the Pre-Gondola I series are presented in Fig. 24. The amplitudes have been plotted according to maximum component velocity and peak resultant velocity for each station. More complete compilations of data are available in Ref. 1 and in Appendix A.

The values designated 'LASA' were derived graphically from recordings of vertical particle displacement obtained from the Large Aperture Seismic Array, which is approximately centered about Miles City, Montana. Although these measurements were not part of the formal data collection program, they are included as a supplement to the intermediate range measurements. These derived particle velocities are probably accurate to not more than ±50%. It should also be noted that they were recorded along a line in a direction opposite to that of the LRL array to the north; however, the generally uniform geology of the region should permit their use as an extension of the LRL data.

STRUCTURES INSTRUMENTATION

The results of the structures instrumentation program are shown in Fig. 25. Peak component amplitudes of structural response are shown for each of the WES stations for the SC-3 and Delta detonations; these two events generally produced the greatest amplitudes of the four shots in each series. More complete tabulations of motions for all events are found in Ref. 2 and in Appendix A. The amplitudes of a low-frequency oscillation (approximately 1.25 Hz) are also plotted for WES station 1. Although not evident on the records of the 1000-lb shots, it is believed that this motion represents a fundamental mode of vibration of the dam. The 1.25-Hz oscillation was very pronounced on the recordings made on the dam; it is not evident on records taken elsewhere. The motion appears to be a resonance effect that builds up and decays a number of times over a span of about 30 sec, with the greatest amplitudes in the horizontal components.

The records from the WES stations for all 20-ton events are very similar with respect to waveforms and frequency content. The seismic signals from the 1000-lb shots were not discernable above the ambient noise level at WES station 2.

In a special test to determine the levels of vibration to which the structure is subjected under normal operating conditions, the control gate at Gate control shaft 3 (WES station 2) was opened to its full aperture and the motion generated by the

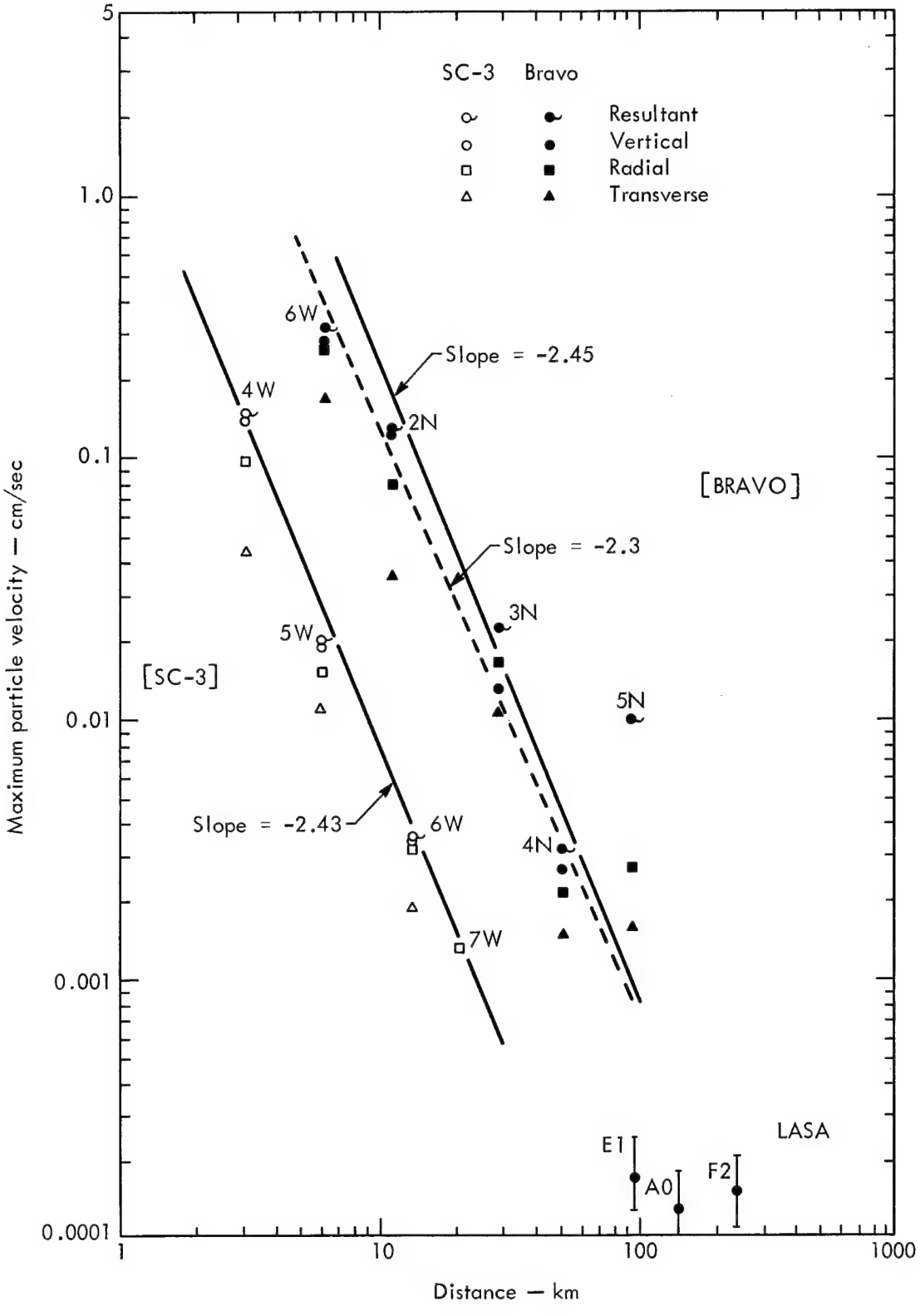

Fig. 24. Results of intermediate range measurements, Bravo and SC-3.

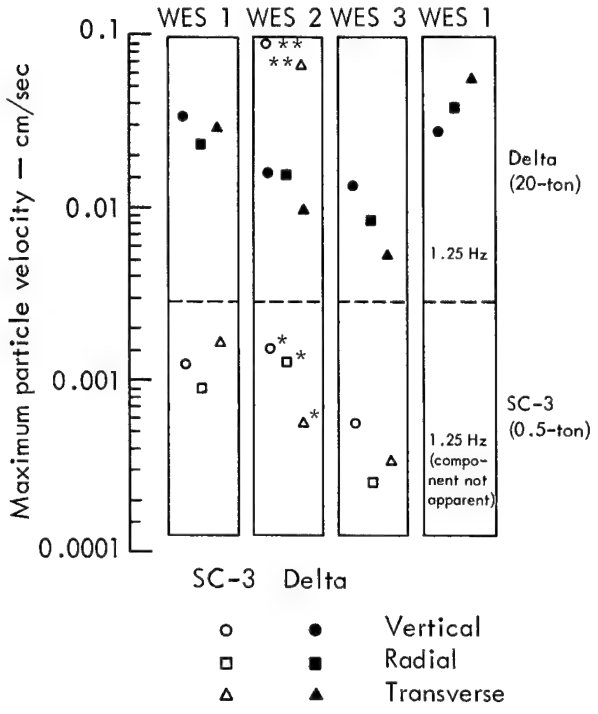

Fig. 25. Results of structures instrumentation, Delta and SC-3.

flow of water was recorded at WES stations 1, 2, and 3. The vibration amplitudes generated by this flow of water were approximately eight times greater at station 2 than the motion induced by the 20-ton charges.

SEISMIC DECOUPLING EXPERIMENT

The results of the seismic decoupling experiment are shown in Fig. 26. Peak component amplitudes of first arrivals and surface waves are shown for both the coupled and the decoupled charges. The ground motion from the decoupled charge was consistently greater than for the coupled charge. It is noted that the charge center for the decoupled charge was at a depth of 17.7 ft or 0.4 ft deeper than the coupled charge depth of 17.3 ft.

For the purpose of comparison, selected amplitudes from the SSC series are used. The SC-2 detonation had a DOB (15.8 ft) closest to the decoupling experiment shots. The amplitudes recorded for SC-2 at WES stations 1 and 3 are shown in Fig. 26. Amplitudes are shown also for the deeper SC-3 Event for LRL station 6W because these were the only data collected at this station.

A prediction for the decoupling experiment shots was made on the basis of the SC-2 recordings at LRL/MSU station 2NE at the crest of the dam. The LRL/MSU data were used for the prediction rather than the corresponding WES data because the LRL/MSU values were higher and were therefore more conservative.

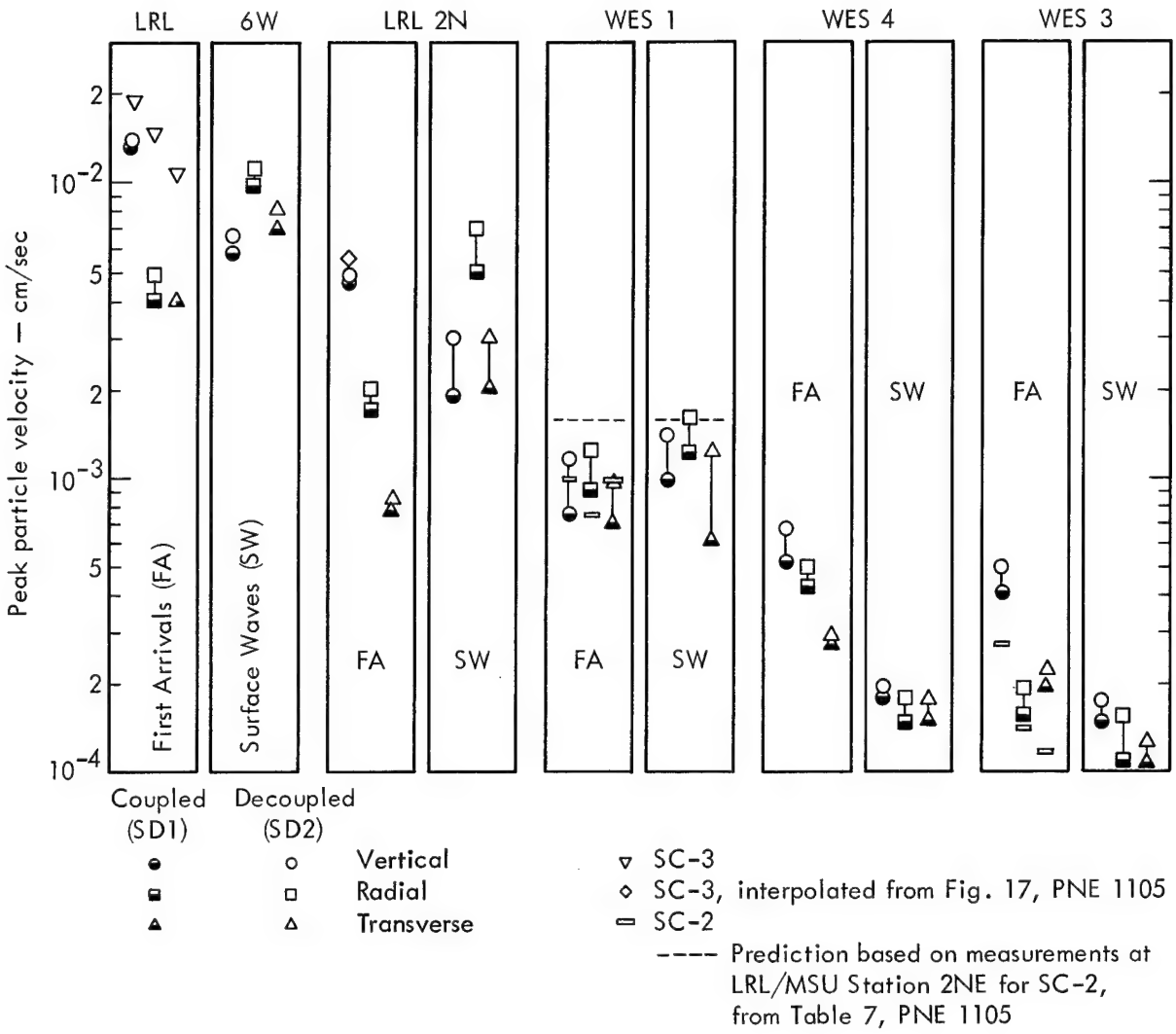

Fig. 26. Results of seismic decoupling experiment.

Analysis of Results

The purpose of this section is to analyze the factors of attenuation, DOB-dependence, and yield scaling as they relate to seismic site calibration. Data are taken from both the intermediate range and structures instrumentation programs.[1,2]

ATTENUATION

The amplitudes from the 1000-lb and the 20-ton events shown in Fig. 24 demonstrate that an inverse power law decay gives a reasonable description of the attenuation of maximum particle velocities with distance; i.e., the amplitudes may be represented by an equation of the form:

$$V_r = CR^{-N}, \qquad (1)$$

where

V_r is the peak particle velocity at a distance R from SGZ

C is a constant whose value is the particle velocity intercept at unit distance

N is an attenuation exponent and is the slope of the line through the data points on a log-log coordinate graph

The following equations apply to the results in Fig. 24:

SC-3 $\quad V_r = 2.3\ R^{-2.43}$ cm/sec (R in km) $\qquad (2)$

Bravo $\quad V_r = 85\ R^{-2.45}$ cm/sec. $\qquad (3)$*

Several interpretations are possible for a visual best fit to the data points, and an alternative for the Bravo points would be:

$$V_r = 27\ R^{-2.3} \text{ cm/sec.} \qquad (4)$$

Generally, the amplitudes decay approximately as $R^{-2.4}$ for both events, but there is some indication that the exponent N may be lower for Bravo than for SC-3.

The peak velocities reported for station 5N are considered anomalous. They are approximately an order of magnitude higher than the velocity intercept of a line through the other points. The velocities at 5N were not taken into account in fitting a line through the data points in Fig. 24. It is possible that the high amplitudes at station 5N may be due to an error in the calibration of the recording instruments.*

DEPTH OF BURST DEPENDENCE

In order to evaluate the effect of the DOB on the coupling of seismic energy, the effects of detonations at the same yield, but at different depths of burial, should be compared at the same recording site. This condition was fulfilled at the WES stations and at LRL station 2N during the 20-ton events. It was partially fulfilled at LRL/MSU station 3 at the base of the dam during the 1000-lb events.

Figure 27 shows the peak resultant amplitudes recorded by the LRL/MSU instruments at the base of the dam for the 1000-lb shots, and also the peak resultant velocities from WES station 1 at the top of the dam. The velocities are plotted

*See Ref. 1.

*Reference to Fig. 29 shows that the resultant velocity at station 5N reported for Bravo is higher than the (preliminary) velocity for the 140-ton row charge, Pre-Gondola II, at the same station.

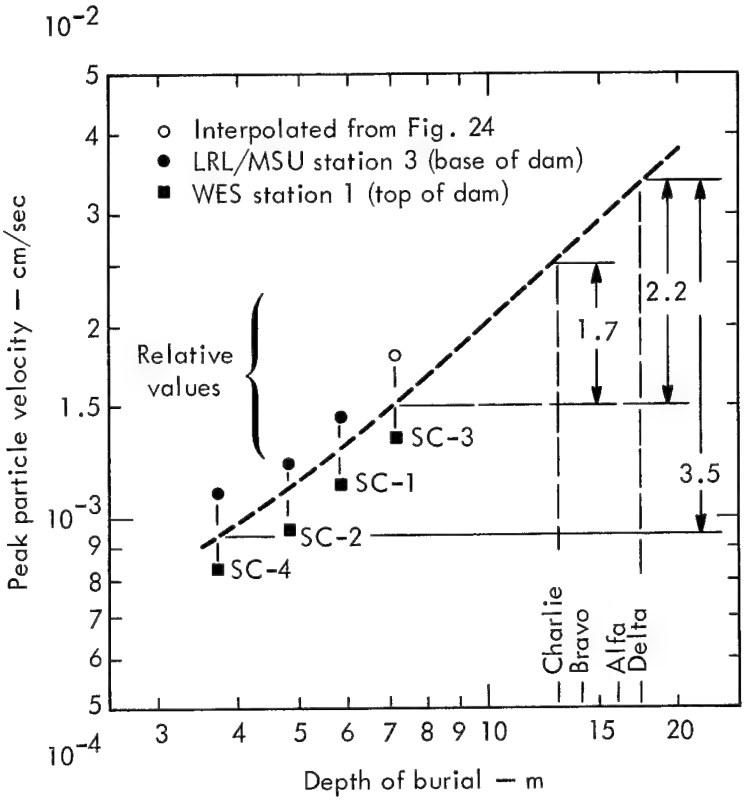

Fig. 27. Relation of peak resultant amplitudes on dam to DOB, Seismic Site Calibration series.

against the corresponding DOBs of the charges. The LRL/MSU value for SC-3 was interpolated from Fig. 24 because there were no recorders at the base of the dam during SC-3. It is evident that seismic coupling increases with DOB for cratering explosions.

Figure 27 can be considered as a graph of scaled particle velocity (i.e., V/W^y, where y is a yield scaling exponent) plotted against DOB. The line drawn through the data points for the 1000-lb charges has been extended to the depths of the 20-ton charges to indicate projected increases in scaled particle velocities for the 20-ton charges compared to the 1000-lb charges. A possible limiting feature of extending the line beyond the data points is that the slope of the line would level off considerably as the depths of the 20-ton charges are approached. Because these depths would be equivalent to containment for charge weights of 1000 lb, the seismic coupling may be approaching a maximum. Also, an extension of the line beyond the 1000-lb amplitudes would be strictly valid only for charges of the same yield.

If it were assumed that the increase in seismic amplitudes due to the greater depth of the 20-ton charges would be approximately in accord with Fig. 27, then this DOB-dependence must be taken into account when estimating the yield scaling. The relative increases in scaled velocities vary from about 1.7 for Charlie compared to SC-3, to about 3.5 for Delta compared to SC-4.

The peak velocities from the 20-ton charges do not show as consistent a relationship to their depth, although there is a definite increase as shown in Fig. 28.

In the preliminary report on the results of Pre-Gondola I,[4] an attempt was made to assign a numerical value to the variation of amplitude with DOB. Within the limited range of depths (D) involved it appeared that the seismic amplitudes varied as $D^{0.86}$.

YIELD SCALING

Several approaches were taken in the evaluation of a yield scaling appropriate to the Pre-Gondola experiments. These methods are discussed below.

If the applicability of an inverse power law attenuation were accepted, then an expedient approach to the determination of yield scaling could be made on the basis

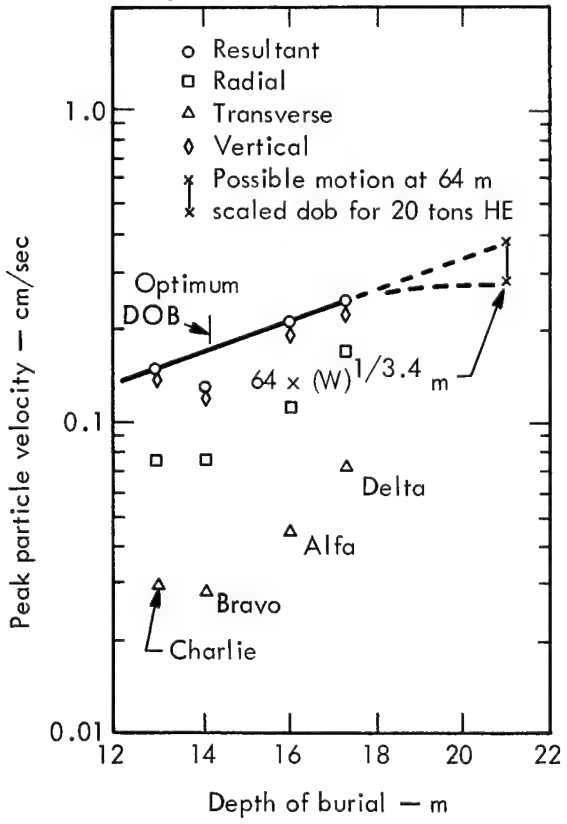

Fig. 28. Peak amplitudes at LRL station 2N (2BN) for Pre-Gondola I.

of a cube root scaling applied to the attenuation exponent obtained from a single yield experiment. This method is used by Mickey, Lowrie, and Shugart.[9] If it is assumed that:

$$V_r \propto (R/W^{1/3})^{-N}, \tag{5}$$

then equivalently

$$V_r \propto W^{N/3} R^{-N}, \tag{6}$$

so that

$$y = \text{yield scaling exponent} = N/3 \tag{7}$$

The average value of N for the Seismic Site Calibration series and the Pre-Gondola I series, based on the values for SC-3 and Bravo of 2.43 and 2.45, would then result in a yield scaling of about 0.81. At the least, this procedure will serve as a guide in adjusting seismograph sensitivities for larger yield experiments at the same test site.

Another approach is to make a direct comparison of the seismic amplitudes (V_1, V_2) from two different yields (W_1, W_2). If recordings are made at the same location, then the following applies:

$$(V_1/V_2) = (W_1/W_2)^y; \tag{8}$$

therefore

$$y = \log (V_1/V_2)/\log (W_1/W_2), \tag{9}$$

where

y is the yield scaling exponent.

The intermediate range and the structures instrumentation programs showed that the average of the peak velocities for all 20-ton events was approximately 30 times that for all 1000-lb events. Because

the yield increase was a factor of 40, the yield scaling would be:

$$y \simeq \log 30/\log 40 \simeq 0.92,$$

neglecting the greater coupling of the 20-ton charges. However, by attributing some of the increase in amplitude to the deeper burial depth of the 20-ton charges, then, for example, a yield scaling based on the average of the peak amplitudes for the three components of first arrivals of energy from Delta and SC-3 at WES station 1 would be:

$$y \simeq \log 24/2.2 \Big/ \log 40 \simeq 0.65,$$

where the factor 24 is the average increase in amplitude (Fig. 25) and 2.2 represents the effect of greater coupling due to the deeper DOB of the 20-ton charge (Fig. 27). This analysis is similar to that of Hankins.[10] If the slope of the line in Fig. 27 levels off as it approaches the depths of the 20-ton charges, which is quite probable, then the yield scaling determined in this manner would be higher than the value of 0.65 above.

In yet another approach to the determination of yield scaling, a value closer to 1.0 was arrived at by Power[1] from a consideration of scaled dobs,* rather than the unscaled depths as used above. He considered that the relative amplitudes from different yields are comparable only if the charges were detonated at the same scaled dob. A scaling factor of $W^{1/3.4}$ was used for the depths, the same scaling which is currently used for crater dimensions.

The peak amplitude at station 5W for Event SC-3 (dob = 64 $m/kt^{1/3.4}$) was compared to a derived amplitude at the same station (6W) for the Pre-Gondola I series. Because none of the 20-ton charges was detonated at a scaled depth of 64 $m/kt^{1/3.4}$, it was necessary to compute what the amplitude at station 6W might have been for a 20-ton charge at this depth.

Figure 28 shows the amplitudes recorded at station 2N for all 20-ton shots. The line through the peak velocities was extrapolated to a depth of 21 m, or 64 $m/kt^{1/3.4}$, and the ratio of the extrapolated velocity (0.37 cm/sec) to the velocity actually recorded for Bravo (0.13 cm/sec) was determined. The peak amplitude recorded at station 6W for the Bravo Event (0.307 cm/sec) was then increased by this ratio, and the result was compared to the amplitude for SC-3 (0.019 cm/sec) at the same location. This method resulted in a yield scaling of:

$$y = \log \frac{(0.37/0.13)(0.307)}{0.019} \Big/ \log 40 = 1.03.$$

Power[1] also considered that the amplitude for the Delta Event (0.25 cm/sec) may have been close to the maximum possible for a charge of 20 tons, and therefore increased the recorded Bravo amplitude at station 6W by the ratio of the Delta to Bravo amplitudes at station 2N. The result was again compared to the amplitude from SC-3 at station 5W:

$$y = \log \frac{(0.25/0.13)(0.307)}{0.019} \Big/ \log 40 = 0.93.$$

The average yield scaling based on the two values above is 0.98.

Because the SC-1 and Delta Events were at approximately the same scaled dob and because there was a recorder at the base of the dam for these two shots, Power[1]

*Lower case letters (dob) indicate scaled depths.

compared the peak amplitudes for these two events to obtain:

$$y = \log (0.035/0.00145)/\log 40 = 0.86.$$

PREDICTIONS FOR PRE-GONDOLA II

The factors discussed in the foregoing sections were taken into account in formulating ground motion predictions for the Pre-Gondola II 140-ton row-charge experiment.

None of the predictions accounted for the frequency of the seismic signal, and only the WES estimates for structural response separated the different components of motion. All of the predictions were based on the assumption that the distributed charge configuration of Pre-Gondola II would behave as a single charge with a yield equal to the sum of the separate charges.

Propagation

For the purpose of setting instrument gains, Power applied an upper limit yield scaling of 1.0 to his equation[1] which represents the results of Pre-Gondola I Bravo. The equation for the attenuation of peak velocities for Bravo was given as:

$$V_r = 85\ R^{-2.45} \text{ (i.e., } V_r = 85 \text{ cm/sec at } R = 1 \text{ km)},$$

so that for a sevenfold yield increase, the intermediate range amplitudes expected for Pre-Gondola II would be:

$$V_r = 85\left(\frac{140}{20}\right)^{1.0} R^{-2.45};$$

therefore,

$$V_r \simeq 600\ R^{-2.45} \text{ cm/sec} \qquad (10)$$

Structural Response

The Nuclear Cratering Group did not give a prediction formula as such, but stated that a yield scaling of approximately 0.67 was applicable.[4] Because the DOBs of the Pre-Gondola II row charges were close to those of Pre-Gondola I, the expected seismic signals from the row charge were $(140/20)^{0.67}$, or about four times the maximum amplitudes recorded during the 20-ton events. The peak motion at WES station 1 was not expected to exceed 0.2 cm/sec.[11]

Ballard[2] used the velocity dependence on depth of $D^{0.86}$ and on yield of $W^{0.67}$ as initially established by NCG[4] and reduced all results of the 1000-lb and 20-ton events to scaled velocities, β, where:

$$\beta = \frac{V}{D^{0.86} W^{0.67}}. \qquad (11)$$

Values of β were plotted against distance from SGZ for each component of motion at the structures instrumentation stations. The line of best fit through the points was used to determine the most probable value of for each station and component. Considering that

$$V = \beta D^{0.86} W^{0.67} \text{ cm/sec} \qquad (12)$$

and substituting the appropriate values of W and D for Pre-Gondola II, he estimated the most probable motions at each station. The maximum probable amplitudes were estimated by using the maximum value of scaled velocity for each component and station. The maximum amplitude at WES station 1 was predicted by Ballard not to exceed 0.21 cm/sec.

PRELIMINARY RESULTS OF PRE-GONDOLA II

Intermediate Range Measurements

The preliminary results of the intermediate range measurements for Pre-Gondola II are shown in Fig. 29. The velocities plotted are preliminary values* of the maximum recorded ground motion, generally in the vertical component. Also shown is the prediction equation $V_r = 600\ R^{-2.45}$. It is apparent that the velocities do not obey the same attenuation pattern as previously observed for the SSC series and Pre-Gondola I. The inverse power law equation for the results is:

$$V_r \simeq 27\ R^{-1.7}\ \text{cm/sec (R in km).} \quad (13)$$

*The preliminary values were obtained by Redpath[7] from the examination of the field playbacks of the magnetic tape recordings.

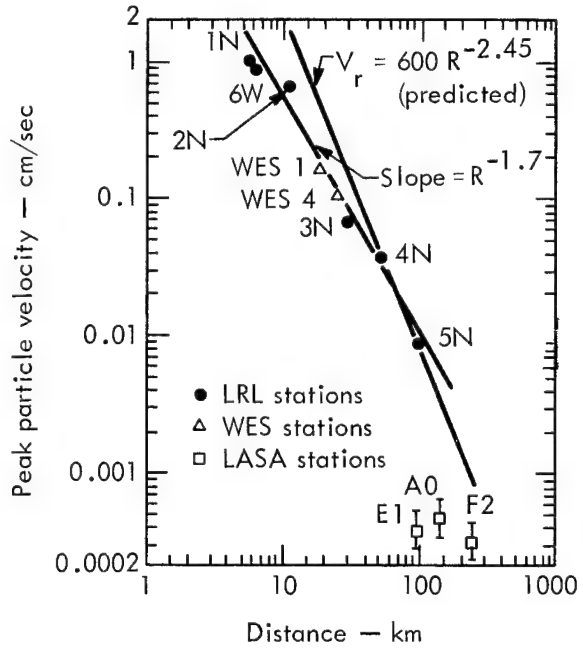

Fig. 29. Preliminary intermediate range measurements, Pre-Gondola II.

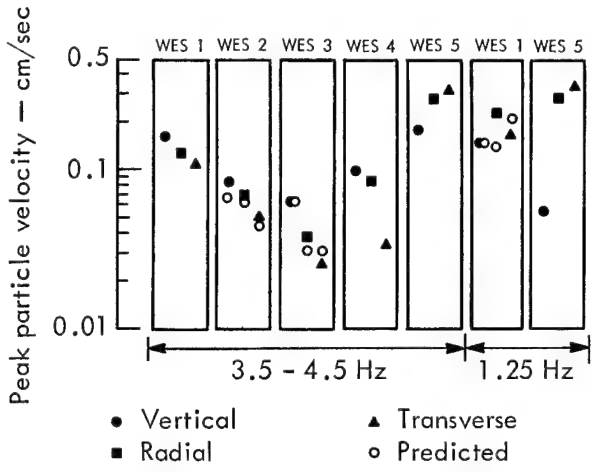

Fig. 30. Preliminary results of structures instrumentation program, Pre-Gondola II.

Increases in amplitude due to the sevenfold step in yield were approximately 0.8 to 14 times the values reported for Bravo[1] which was at a lesser DOB. However, the Bravo data are the only amplitudes for a 20-ton shot which were recorded at the intermediate range stations, and with which a comparison can be made.

Structures Instrumentation

The preliminary results[12] of the measurements at the structures instrumentation stations are shown by component in Fig. 30 together with the amplitudes predicted by Ballard.[2]

The amplitudes generated by the 140-ton row charge at the WES stations were approximately 3.3 to 6.6 times greater than those from Alfa, the 20-ton charge with a DOB comparable to the row charges. The average increase was 4.8 times, which indicates a yield scaling factor near 0.8 according to Eq. (9).

The maximum velocity of 0.23 cm/sec measured at the top of the dam was close

to the maximum velocity of 0.21 cm/sec predicted by Ballard.[2]

The only significant output of the hydrophone in the reservoir was a pressure pulse of 7.5×10^{-3} psi which arrived at approximately the same time as the peak compressional energy at WES station 1. This pressure pulse would correspond to energy refracted into the water from the reservoir bottom. A direct transmission of energy through the water, which would be distinguished by a time of arrival corresponding to an apparent velocity of about 5000 ft/sec (i.e., water velocity), was not observed.

Discussion and Interpretation of Results

This section follows the current practice of presenting the theory of seismic wave propagation and effects by discussing separately the source mechanism, the transmission characteristics of the region, and the response of structures of interest.

SOURCE

Depth-of-Burst Dependence

The results of the Seismic Site Calibration series and Pre-Gondola I demonstrate that the seismic coupling of explosive energy is very dependent upon the DOB of the charge. An approximate graphical or empirical formulation of this dependence was found for the limited range of depths and yield of the Pre-Gondola experiments, but a meaningful extension of this relationship to deeper depths and larger yields has not been established. Power[1] refers to the significance that the DOB-dependence may have upon damage predictions for cratering explosions based upon data from contained explosions. He states that such cratering predictions could be high by as much as a factor of two.

Yield Scaling

The values of the yield scaling exponents that were estimated by the various agencies differed, as did their approach to the yield scaling evaluation. The value of 0.67 as originally proposed by NCG is probably too low, and the value of about 1.0 proposed by Power[1] is probably too high. A yield scaling exponent between 0.7 and 0.8 is the best estimate that can be made at this time for the range of HE yields and cratering DOBs at Fort Peck.

Theoretical investigations by Peet[8] show that yield scaling is not a single valued parameter, but is a function of the yield and the frequency of the signal at which it is measured. Peet states that the yield scaling exponent varies from a maximum value of 4/3 for frequencies near zero to a value of 1/3 for high frequencies. He suggests that the maximum amplitude of the signal spectrum of an explosion varies as $W^{2/3}$, and the frequency of this peak in the spectrum varies as $W^{-1/3}$. If this were the case, then the value of N in an attenuation equation of the type $V_r = CR^{-N}$ would decrease as the yield increases. The predominant frequency of the seismic energy spectrum decreases as the yield goes up, and the lower frequencies are attenuated less than the high. The source spectrum is discussed later under the heading, "Estimation of Seismic Amplitude Spectrum."

Seismic Effect of Row-Charge Configuration

From the preliminary results of Pre-Gondola II, it appears that the distributed row-charge configuration generated ground motion amplitudes equivalent to a single charge of the same total yield. This might not be the case for a long row in which the length is many times that of a single crater radius.

There does not appear to be any asymmetry of seismic energy radiation with respect to alignment of the row at the Pre-Gondola site, but there is also very little evidence on which to base a definite conclusion. Intuition suggests that a row might appear as a point source of energy

at distances which are large compared to the dimensions of the row, and that asymmetries of energy radiation would not be distinguishable from asymmetries in the transmission characteristics of the surrounding region, or from the influence of overburden differences between recording sites.

Decoupling Experiment

The results of the seismic decoupling experiment in Fig. 26 show that the charge fired in the decoupling cavity consistently generated higher seismic amplitudes than did the fully coupled charge.[5]

This unexpected difference in amplitudes cannot be explained by the fact that the decoupled charge was buried 0.4 ft deeper than the coupled charge. According to Fig. 27, this would result in only a 5% increase (approximately) in seismic amplitudes, whereas Fig. 26 shows that the increases were as much as 50%. It had been expected that the decoupled charge would generate slightly lower amplitudes than the coupled charge.

TRANSMISSION CHARACTERISTICS OF REGION[7]

This section will discuss the intermediate range measurements with respect to the general validity of the inverse power law equation, and to a more physically realistic frequency-dependent form of propagation equation. An attempt will be made to show that the Pre-Gondola data obey a frequency-dependent attenuation, and that this form of propagation equation can lead to a more meaningful analysis of the data, including an estimate of the primary frequency content of the seismic source.

Applicability of Inverse Power Law Attenuation

The attenuation patterns observed for the 1000-lb and the 20-ton detonations were approximately the same according to Power.[1] Other interpretations are possible in fitting a line to the data points in Fig. 24. For example, a line with a slope of N = -2.3 also gives a reasonable fit to the Bravo data points.

In general, an inverse power law gives an adequate description of the decay of maximum seismic amplitudes for intermediate ranges for the SC-3 and Bravo Events, with the provision that a lower value of N will describe the Bravo Event. A power law relation also fits the preliminary results of Pre-Gondola II reasonably well, but the slope of the line is less than that for either of the other two series. This suggests a variation of N with yield, in keeping with the suggestions made at the outset of this section under the heading "Yield Scaling." The same inverse power law exponent does not appear to be applicable to events of different yield at the Pre-Gondola test site.

There is justification for assuming the applicability of an experimental law such as $V_r = CR^{-N}$ only because it generally describes the maximum recorded amplitudes reasonably well, at least for intermediate ranges from the seismic source. This equation for the attenuation of peak amplitudes is commonly used by most investigators to describe the propagation of ground shock from conventional or nuclear explosions. The equation has the advantage of a simple and straightforward formulation; however, it cannot account for the frequency content of the seismic signal, and different values of N are often required to

give a full description of the amplitudes over a large distance. The indications, both theoretical and experimental, that N varies with yield is a further limitation upon use of this formula for predicting the effects of higher yields.

Frequency-Dependent Attenuation

An equation with a more realistic physical basis than an inverse power law for the attenuation of seismic energy is an expression with two terms involving distance, one for geometrical spreading and the other for attenuation of energy due to loss mechanisms such as friction.

If the attenuation of seismic energy is proportional to the first power of the frequency, as has been shown by several experimental investigations,[13,14] then the decay of amplitudes in a homogeneous medium will be according to[15,16]:

$$V_r = V_0(R/R_0)^{-A} e^{-kf(R-R_0)}, \quad (14)$$

where

V_r is the particle velocity at a distance R from the source

V_0 describes the particle velocity amplitude spectrum at a distance R_0 from the source

R_0 is an arbitrary distance from the source

A is an exponent which would have the value of one for body waves and one-half for surface waves

f is the frequency of the signal

k is an attenuation operator for the medium = π/Qc sec/km

Q is an attenuation constant for the medium

c is the propagation velocity

The term $(R/R_0)^{-A}$ accounts for geometrical spreading (i.e., spherical or cylindrical divergence), and the exponential term accounts for the losses due to attenuation.

A simple model of the Fort Peck area is not homogeneous, but rather a horizontally stratified geologic situation. The travel times of the maximum amplitude signals were determined from the approximate zero time which was recorded on the seismic records of Pre-Gondola II by the station operators, and these times are plotted in Fig. 31. The maximum particle velocities have an apparent propagation velocity of about 2.4 km/sec, compared to an apparent velocity of 6.4 km/sec for the first arrival of energy, and approximately 0.9 km/sec for the lower frequency surface waves. The surface waves are dispersive. The comparatively low velocity of 2.4 km/sec would indicate that the maximum amplitudes are transmitted almost entirely along a surface layer, and therefore they would diverge cylindrically. For the case of cylindrical spreading, A = 0.5, and Eq. (14) becomes:

$$V_r = V_0 (R/R_0)^{-0.5} e^{-kf(R-R_0)} \quad (15)$$

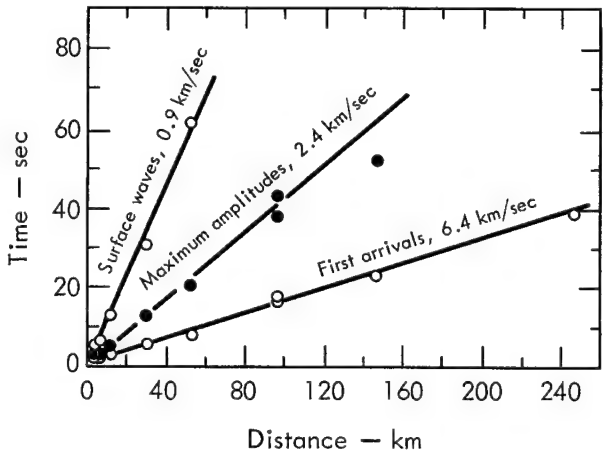

Fig. 31. Travel times for Pre-Gondola II.

Equation (15) should describe the propagation of maximum amplitudes at the Fort Peck site.[7]

Experimental Verification of Frequency-Dependent Attenuation

In order to make use of Eq. (15), the value of the attenuation operator k must be known. The value of k can be determined from the intermediate range field measurements in the manner described in the following paragraphs.

Because the intermediate range amplitudes are normally plotted against distance on a log-log coordinate graph, it is convenient to put Eq. (15) into logarithmic form:

$$\ln V_r = \ln V_0 - 0.5 \ln (R/R_0) - kf(R - R_0), \quad (16)$$

differentiating $\ln V_r$ with respect to $\ln R$:

$$-\partial \ln V_r / \partial \ln R = -\partial \log V_r / \partial \log R = 0.5 + kfR. \quad (17)$$

The term $\partial \log V_r / \partial \log R$ is the slope of a line through the intermediate range data points. Designating this slope -p:

$$p = 0.5 + kfR; \quad (18)$$

therefore,

$$k = (p - 0.5)/fR.$$

It follows that k can be evaluated by measuring the slope p of the observed attenuation curve at a distance R, and substituting this value together with the observed frequency of the seismic signal, f, into Eq. (18).

Prior to evaluating k from the Pre-Gondola data, it may be appropriate to give an idealized representation of the foregoing discussion. Figure 32 shows a series of attenuation curves for a few discreet frequencies; in a real case, there would be a continuum of curves for an infinite number of frequencies. The upper bound of the amplitudes can be described by a curve which is tangent to the separate curves, and which would represent the attenuation of peak amplitudes actually measured in an intermediate range program, providing the recording instruments had sufficient response. The velocities at R_0, which are V_0, will depend on the shape of the amplitude spectrum curve.

Assuming that the maximum amplitudes propagate along a surface layer and that Eq. (15) is valid, then the Pre-Gondola data should fit the assumptions. The data collected during Pre-Gondola II were selected as a test.

Figure 33 is a plot of the preliminary results of Pre-Gondola II. It is the same as Fig. 29 with the addition of a smooth curve drawn as an approximate visual fit to the data points, including the velocities derived from the LASA displacement recordings. The curve through the data points corresponds to the upper bound of amplitudes illustrated in Fig. 32. Some of the scatter about the curve is attributed to differences in conditions at the recording sites.

To evaluate k, the slope of the curve in Fig. 33 was measured at each distance, R, corresponding to a recording station, and the frequencies of the observed maximum signals were estimated from the field playbacks of the magnetic tape recordings. These values were substituted into Eq. (18). The following values apply:

Station	R (km)	f (Hz)	p	k = (p - 0.5)/fR (sec/km)
6W	6.4	9.0	1.22	0.0125
2N	11.6	5.5	1.45	0.0150
WES1	18.5	4.5	1.72	0.0146
WES4	24.8	3.5	1.89	0.0159
3N	29.3	3.2	2.06	0.0163
4N	52.0	3.2	2.92	0.0146
5N	95.9	2.6	4.39	0.0155
			Average	0.0150

Data from LRL station 1N are not included because the frequency of the signal could not be determined from the field playback record, and data from WES stations 2, 3, and 5 are not included because the transducers at these stations were mounted on concrete or steel, possibly leading to distortion of the seismic signal.

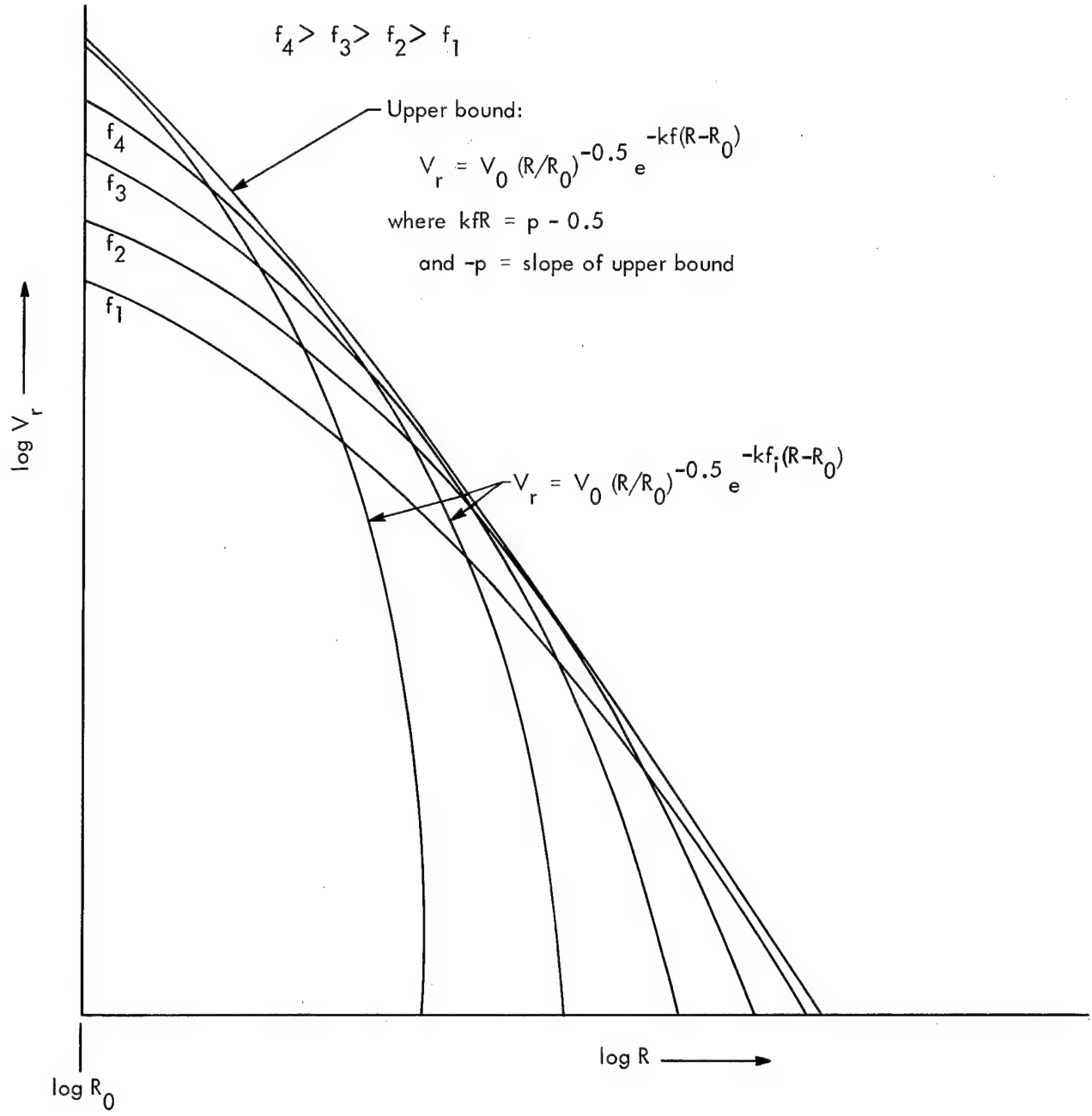

Fig. 32. Idealized representation of attenuation curves and their upper bound (Ref. 7).

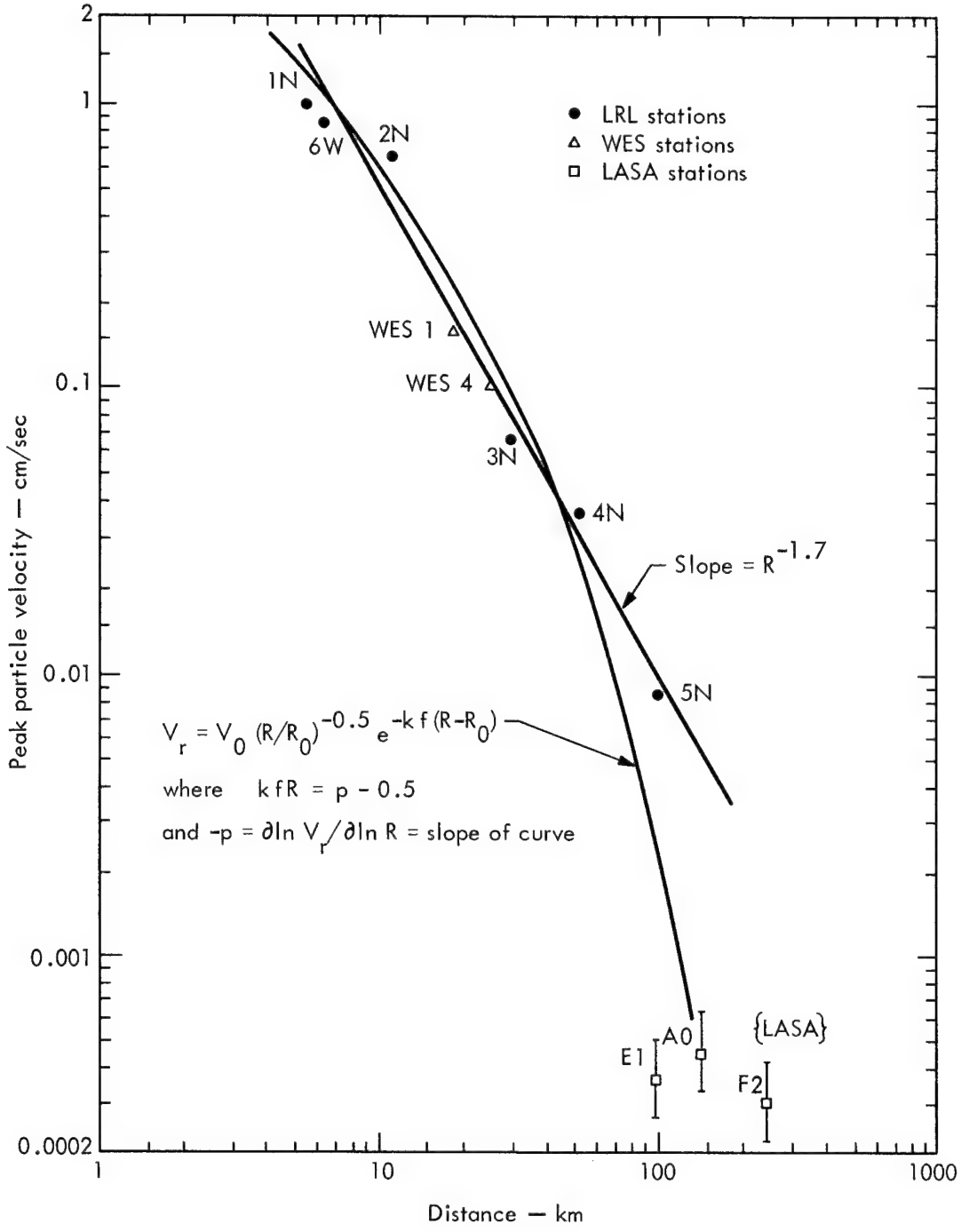

Fig. 33. Smooth curve fit to preliminary intermediate range measurements from Pre-Gondola II (Ref. 7).

The fairly consistent values of k determined at each distance lend support to the use of Eq. (15) to describe the propagation of peak seismic amplitudes at the Fort Peck site. One would expect the value of k to remain reasonably constant with distance if the maximum amplitudes are transmitted along a continuous surface layer. There is some suggestion that a waveguide type of propagation may exist. In contrast, if the maximum signals had refracted through a number of different

geologic strata, then one might expect the value of k to vary with distance.

The value of k = 0.015 sec/km determined above appears to be reasonable, although it is lower than most values reported in Ref. 13 for a variety of rock types. This value of attenuation can also be expressed as $1.5 \times 10^{-7} f$ dB/cm. As a comparison, k = 0.045 sec/km for the Pierre shale of Colorado,[14] and Q = π/kc = 90 for Bearpaw shale (c = 2.4 km/sec), compared to Q = 70 reported for Sylvan shale in Table 3-1 in Ref. 16.

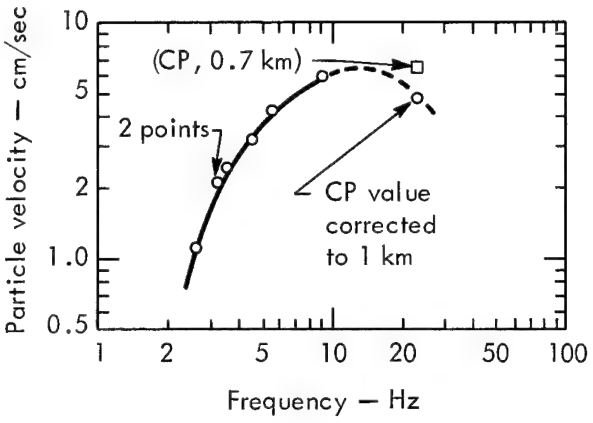

Fig. 34. Derived values of V_0 for R_0 = 1 km (Ref. 7).

Estimation of Seismic Amplitude Spectrum

If the foregoing discussion and analysis of the attenuation of peak seismic signals were valid, the following method is suggested for the determination of the variation of maximum seismic amplitudes with frequency at a point close to the source.

The attenuation equation, Eq. (15), may be rewritten as:

$$V_0 = V_r (R/R_0)^{0.5} e^{kf(R-R_0)}, \qquad (19)$$

and values of V_0 for Pre-Gondola II can be computed from the curve in Fig. 33 by using corresponding values of R, V_r, the observed frequencies of the maximum signals, and the average value of k of 0.015 sec/km. The following values apply to evaluation of V_0 at a distance of 1 km (i.e., R_0 = 1 km):

Station	V_r (from curve) (cm/sec)	R (km)	f (Hz)	$V_0 = V_r R^{0.5} e^{kf(R-1)}$ (cm/sec)
6W	1.1	6.4	9.0	5.8
2N	0.52	11.6	5.5	4.2
WES1	0.23	18.5	4.5	3.2
WES4	0.14	24.8	3.5	2.4
3N	0.10	29.3	3.2	2.1
4N	0.025	52.0	3.2	2.1
5N	0.0028	95.9	2.6	1.1

The values of V_0 are plotted against frequency in Fig. 34, which would then be a partial spectrum of peak seismic energy based on intermediate range measurements of seismic amplitudes. The value of V_0 plotted at 23 Hz was derived from a WES recording of vertical ground acceleration at the Pre-Gondola CP trailer.[6] The acceleration was nearly sinusoidal, facilitating conversion to particle velocity according to simple harmonic motion. The derived velocity was corrected to a distance of 1 km from the source by means of Eq. (15), with R = 1.0 km and R_0 = 0.7 km (the CP trailer was approximately 0.7 km from the Pre-Gondola II crater).

The information in Fig. 34 may in turn be used to compute a spectrum of the maximum ground motion at any distance by means of the attenuation equation, Eq. (15). For example, Fig. 35 is the derived spectrum at the Fort Peck Dam. It was computed by assuming R = 18.5 km, and by using the values of V_0 in Fig. 34 at arbitrarily selected frequencies.

The foregoing derivation of the near source spectrum is somewhat artificial in the sense that a curved line fit to the data points is used rather than the actual recorded values of V_r. (Computations of the

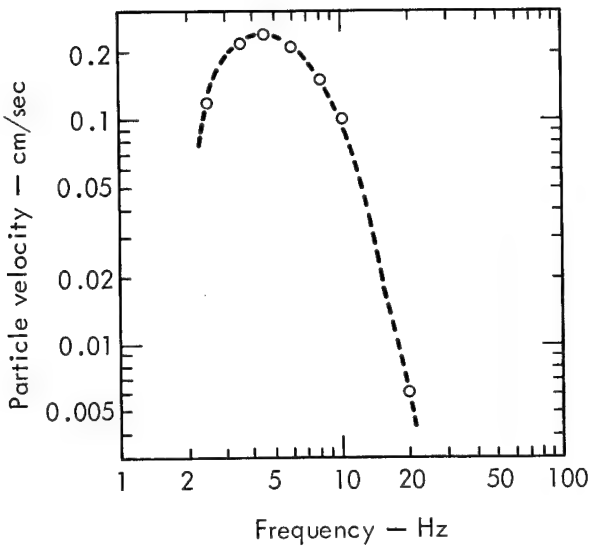

Fig. 35. Spectrum of peak ground motion at Fort Peck Dam (R = 18.5 km), derived from Fig. 34 (Ref. 7).

amplitude spectrum with the recorded values resulted in a more irregular plot of V_0 vs f, although the trend of values is still the same.) Local conditions at the recording sites can be expected to produce magnification or diminution of the ground motion amplitudes above and below the general trend of values. It is believed that smoothing the amplitude-distance plot by means of a smooth curve through the data points does not render the method invalid.

In support of the above method for estimating the amplitude spectrum, it is interesting to note that the peak of the particle velocity curve in Fig. 34 occurs at about 14 Hz. This value is in accord with a consideration of the length of the Pre-Gondola II row-charge detonation (approximately 500 ft), and the measured compressional wave velocity of the shale medium at the site (6800 ft/sec).[4] If the predominant wavelength of the seismic pulse were considered equal to the length of the row, then the predominant frequency would be 6800/500, or about 14 Hz. This argument corresponds to Peet's suggestion[8] that the frequency of the maximum shock from an explosion is proportional to $W^{-1/3}$; in the case of a single charge the linear dimensions of the cavity or crater will vary approximately as $W^{1/3}$.

When comparing row-charge detonations, Redpath believes that the known spectrum for a row charge with length L_1 can be used to estimate the spectrum of another row with length L_2 by shifting the frequency of the spectral peak by a factor of L_1/L_2, rather than by the cube root of the ratio of the yields.[7] This follows from his hypothesis that the length of a row charge, not its total yield, largely determines the predominant frequency of the seismic pulse. The length of a row can be considered as the distance between points one single-charge crater radius beyond the end charges. This hypothesis would probably not hold true for very long rows.

It is also interesting to compare the derived peak particle velocity observed at the CP of 6.8 cm/sec (at 0.7 km) to the values predicted for a distance of 1 km from SGZ of Pre-Gondola II by the various equations which have been discussed. Equation (15), as manifested in Fig. 34, predicts that the peak velocity at 1 km would be 6.5 cm/sec, whereas Eq. (13) based on the observed attenuation for Pre-Gondola II would predict 27 cm/sec, and Eq. (10) based on the SSC series and Pre-Gondola I would predict 600 cm/sec. The high velocities predicted by the inverse power law equations confirm that the use of this type of equation should be limited to intermediate ranges only.

The amplitude spectrum in Fig. 35 and its method of derivation could be tested by

comparison with a harmonic analysis of the peak ground motion recorded at the base of the Fort Peck Dam, as planned by Power.[17]

Directional Asymmetry of Propagation

The existence of directional asymmetry to the propagation of seismic energy through the medium around the test site is not apparent from the information collected for any of the Pre-Gondola events. As previously mentioned, a scatter of the recorded peak amplitudes would be expected due to variations in local geology from recording site to recording site. The determination of any asymmetry would require a considerable number of seismographs well distributed about the test site.

STRUCTURES RESPONSE

Good documentation was obtained for the response of those structures which were instrumented during the Pre-Gondola experiments. The recorded response of the individual structures was generally very similar for the different series. It is believed that this reflects primarily on the modes of response of the structure rather than on the frequency content of the energy generated by the explosions. An exception is that the 1000-lb charges did not excite the pronounced 1.25-Hz motion of the dam that was observed during Pre-Gondola I and II. There was no evidence of any damage or change to any portion of the structures.

PREDICTIONS FOR FUTURE CRATERING EXPERIMENTS

In order to illustrate the application of the concepts just presented under the heading, "Transmission Characteristics of Region," predictions will be made for possible row-charge designs of 100-ton, 140-ton, and 230-ton total yield. It is assumed that the row will consist of either five or seven main charges.

Prediction Using Frequency-Dependent Attenuation

In order to use the propagation equation, Eq. (15), to predict the variation of maximum seismic amplitudes with distance, it is first necessary to predict how the frequency of the peak seismic signal will vary with distance. This section suggests a method of estimating the variation of the frequencies of the maximum ground amplitudes as a function of distance. This method will then be applied to the Pre-Gondola II data in order to predict the effects of the hypothetical experiment.

The frequencies of maximum ground motions are estimated in the following manner. At a distance R the peak value of V_r will occur at that frequency for which:

$$\partial V_r / \partial f = 0, \tag{20}$$

or equivalently

$$\partial \ln V_r / \partial \ln f = 0; \tag{21}$$

so that from Eq. (15):

$$\partial \ln V_r / \partial \ln f = \partial \ln V_0 / \partial \ln f - kf(R - R_0) = 0; \tag{22}$$

therefore,

$$\partial \ln V_0 / \partial \ln f = kf(R - R_0).$$

The term $\partial \ln V_0 / \partial \ln f$ is the slope, m, of

the amplitude-frequency curve at any frequency f. Therefore:

$$m = kf(R - R_0)$$

or

$$R = (m/kf) + R_0 \qquad (23)$$

where R_0 is the distance from the seismic source at which the amplitude spectrum, V_0, is defined. It follows that the expression $(m/kf) + R_0$ is equal to the distance at which the frequency of the maximum ground motion is f, m being evaluated at f.

The Pre-Gondola II row consisted of both 40- and 20-ton charges and had a length of about 500 ft. Similarly, the length of a row of five 20-ton charges would be 480 ft, and the length of a seven charge row should be 640 ft. These lengths assume a charge spacing of one crater radius, 80 ft.

Assuming the validity of the earlier discussion under the heading, " Estimation of Seismic Amplitude Spectrum," it follows that the peak of the curve in Fig. 34 would have a negligible horizontal frequency shift for a 100-ton row, and a shift of 500/640 = 0.78 × for a seven-charge row. According to the earlier discussion, the amplitude of the peak particle velocity would not be shifted for a 140-ton row, but for a 100-ton row it would be lowered by $(100/140)^{0.67}$ = 0.80 ×. Figure 36 shows the curve in Fig. 34 shifted by these amounts, while the shape of the curve has been maintained.

140-ton Row. To predict the effects for the 140-ton row, Eq. (23) is applied to the shifted amplitude-frequency curve by measuring slopes at a number of arbitrarily selected frequencies and evaluating (m/kf) + 1. The following values apply:

f (Hz)	m	V_0 (cm/sec)	(m/kf) + 1 = R (km)
2	3.7	0.96	124
3	1.6	2.5	37
4	1.0	3.6	18
5	0.85	4.5	12
6	0.64	5.2	8
7	0.53	5.6	6
9	0.25	6.2	3
11	0.0	6.5	1

The values of f, R, and V_0 are substituted into Eq. (15) to compute the values of V_r. To give the prediction for a 140-ton seven-charge row, V_r is plotted against distance in Fig. 37.

Five-charge 100-ton Row. Because the amplitude spectrum for the 100-ton five-charge row is changed only in amplitude, the prediction for this row will be the same as in Fig. 33, but everywhere lowered in amplitude by 0.80 ×. This new curve is shown in Fig. 37.

Alternate Designs. An alternative design could be one equal in length to a seven-charge 140-ton row, but with greater equivalent yield at any given cross section. To illustrate the prediction procedure, assume the total yield to be 230 tons. The

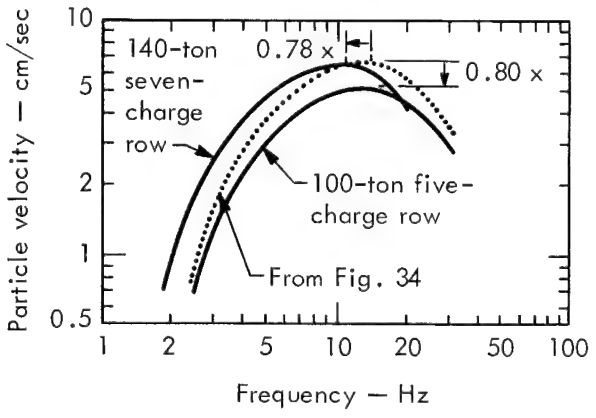

Fig. 36. Shift of amplitude-frequency curve for 100-ton and 140-ton row charges (Ref. 7).

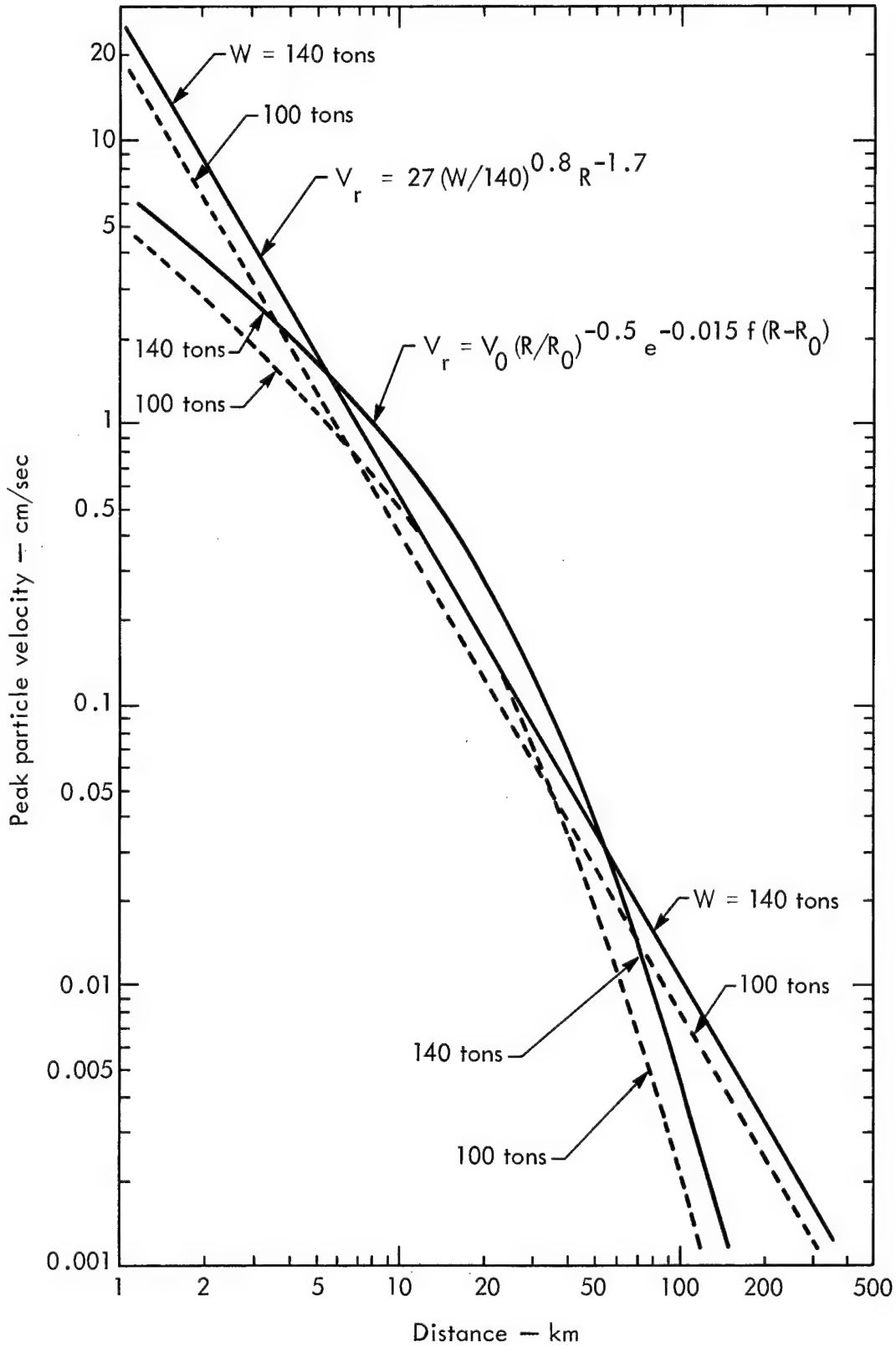

Fig. 37. Example of intermediate range predictions for row-charge cratering experiments (Ref. 7).

frequency content of the seismic pulse should not differ greatly from the 140-ton row, because their lengths are equivalent, but the seismic amplitudes should be higher by the factor of $(230/140)^{2/3} \simeq 1.4$. Consequently, the prediction curve in Fig. 37 for the seven-charge 140-ton row based on frequency-dependent attenuation could be used to predict the effects of the 230-ton array by shifting the curve up in amplitude by 40%.

Inverse Power Law Predictions

The inverse power law equation of the line through the Pre-Gondola II data points in Fig. 29 is:

$$V_r \simeq 27R^{-1.7}; \tag{24}$$

so that, assuming a yield scaling exponent of 0.8 is applicable to the inverse power law formulation, the prediction equation for another experiment in inverse power law form would be:

$$V_r \simeq 27 \left(\frac{W}{140}\right) R^{-1.7}, \tag{25}$$

where W is the total yield of the other experiment.

Figure 37 shows the predictions based on Eq. (25) for yields of 100 and 140 tons. The prediction for 140 tons is the same line as drawn through the observed values in Fig. 29. The equation may be used for predictions for any other yield.

Conclusion and Recommendations

Based on the results of the seismic studies to date, the following conclusions are drawn.

SOURCE

Figures 27 and 28 show that the amount of seismic energy coupled to the surrounding medium is very dependent upon the DOB of the charge, a factor which should be taken into account when the seismic effects of cratering explosions are predicted.

A value of 0.8 appears to be appropriate for the yield scaling exponent for HE cratering detonations at the Fort Peck site if an inverse power law is used to predict seismic effects. There are theoretical indications, supported by the Pre-Gondola intermediate range results, that the yield scaling exponent is not a single-value parameter, but depends on the yield of the explosion and the frequency of the signals being compared.

The distributed row charge apparently generated seismic amplitudes equivalent to a single charge with the same total yield.

No asymmetry of radiation from the row was noted, but there is insufficient evidence on which to base a conclusion. A distribution of recorders around the row at close ranges would be required to measure any radiation asymmetry.

There is no apparent reason why the decoupled charge of the seismic decoupling experiment generated greater seismic amplitudes than the fully coupled charge.

TRANSMISSION CHARACTERISTICS OF REGION

An inverse power law provides a sufficient description of the attenuation of peak seismic particle velocities for intermediate ranges, although the same attenuation exponent cannot be applied to single 20-ton cratering charges and to a large-yield distributed row charge with individual charges of approximately the same yield. The value of N in the equation $V_r = CR^{-N}$ varies from about 2.3 to 2.5 for the SSC series and Pre-Gondola I to 1.7 for Pre-Gondola II.

A propagation equation which includes a term for geometrical divergence and an exponential term for attenuation losses presents a more physically realistic formulation of the overall decay of seismic energy with distance. The data from Pre-Gondola II appear to fit this type of propagation law. This formulation implies that the apparent attenuation rate will decrease as the yield increases because a greater portion of the energy is contained in lower frequency signals which are attenuated less than the higher frequencies per unit distance.

It seems probable that the larger dimensions and yields of the row charge generated a different spectrum of seismic energy compared to the single-charge cratering experiments. It is suggested that the larger dimensions and yield shifted the source spectrum towards lower frequencies, and that this is why the apparent attenuation rate for Pre-Gondola II was less than for the smaller yield detonations.

The maximum amplitudes appear to propagate along a comparatively low-velocity surface layer, with the possibility that some waveguide type of propagation may exist. If so, then the Bearpaw shale formation is probably the guiding layer.

A relatively insignificant amount of seismic energy is transmitted through the Fort Peck Reservoir.

There are insufficient data to arrive at a conclusion regarding asymmetry of seismic energy propagation in the area.

STRUCTURES INSTRUMENTATION

The results of the structures instrumentation program show that this program, as implemented, is adequate to monitor the vibration of the important structures of interest in the area. The motions recorded at the structures were below damage thresholds.

PREDICTIONS FOR FUTURE HE TESTS AT FORT PECK

From the preliminary results of Pre-Gondola II, it appears that a simple extension of the attenuation data obtained for the previous 1000-lb and 20-ton experiments did predict the motion generated by the row charge within acceptable limits of error.

At the present time it appears, however, that a separate inverse power law prediction scheme is preferred for each event at a different yield level. Using the appropriate attenuation and DOB-dependence, the yield scaling exponent of 0.8 should provide a reasonably accurate estimate of maximum seismic amplitudes, provided that future experiments are not significantly beyond the range of present experience. Equation (25) should adequately predict the intermediate range effects of events near the 140-ton yield level

A knowledge of the dependence of the seismic source spectrum upon yield and charge configuration, together with a frequency-dependent attenuation equation, would allow more reliable estimates of the amplitude and frequency of seismic signals.

According to the results of the experiments performed at Fort Peck, an extension of the existing inverse power law equations to events of higher yield would predict the seismic effects sufficiently well. However, the general applicability of an inverse power law formulation for the attenuation of seismic amplitudes is suspect, especially when attempts are made to extrapolate the information from comparatively small-scale HE tests to the yields conceived of as necessary for nuclear excavation projects.

RECOMMENDATIONS

It is recommended that future programs of seismic monitoring of cratering or contained explosions be designed to subject the data to a complete analysis, including spectral analysis and determination of travel times, and that attempts be made to apply this information to a more physically realistic treatment of energy propagation than the inverse power law.

References

1. D. V. Power, Project Pre-Gondola I - Intermediate Range Ground Motions, Lawrence Radiation Laboratory, Livermore, Rept. PNE-1105, July 1967.
2. R. F. Ballard, Jr., Project Pre-Gondola I - Structures Instrumentation, U. S. Army Engineer Waterways Experiment Station, Vicksburg, Mississippi, Rept. PNE-1106, August 1967.
3. W. W. Dudley and H. A. Jack, Project Pre-Gondola - Site Selection Investigations, U. S. Army Engineer Nuclear Cratering Group, Livermore, Rept. PNE-1101, February 1967.
4. M. K. Kurtz, A Report of the Scope and Preliminary Results of Project Pre-Gondola I, U. S. Army Engineer Nuclear Cratering Group, Livermore, Rept. NCG/TM 66-20, 9 December 1966.
5. R. W. Harlan, W. G. Christopher, and B. B. Redpath, Pre-Gondola Seismic Decoupling Series, U. S. Army Engineer Nuclear Cratering Group, Livermore, Rept. NCG/TM 67-10, July 1967 (Revised January 1968).
6. M. K. Kurtz, A Report of the Scope and Preliminary Results of Project Pre-Gondola II, U. S. Army Engineer Nuclear Cratering Group, Livermore, Rept. NCG/TM 67-9, 14 August 1967.
7. B. B. Redpath, Concept and Techniques of Seismic Site Calibration for Project Pre-Gondola, U. S. Army Engineer Nuclear Cratering Group, Livermore, Rept. NCG/TM 67-19, 12 December 1967.
8. W. E. Peet, "A Shock Wave Theory for the Generation of the Seismic Signal Around a Spherical Shot Hole," Geophys. Prospecting, 8, 509 (1960)
9. W. V. Mickey, L. M. Lowrie, and T. R. Shugart, Earth Vibrations from a Nuclear Explosion in a Salt Dome, Project Dribble Salmon Event, Coast and Geodetic Survey, Rockville, Maryland, Rept. VUF-3014, 17 March 1967.
10. D. M. Hankins, Seismic Data from High Explosive Cratering Tests at Nevada Test Site, Sandia Corporation, Albuquerque, Rept. SC-4693(RR), April 1963.
11. M. K. Kurtz, Technical Director's Operation Plan - Project Pre-Gondola II, U. S. Army Engineer Nuclear Cratering Group, Livermore, 17 May 1967.
12. R. F. Ballard, Jr., U. S. Army Engineer Waterways Experiment Station, private communication, 20 July 1967.
13. P. B. Attewell and Y. V. Ramana, "Wave Attenuation and Internal Friction as Functions of Frequency in Rocks," Geophysics 31, 1049 (1966).
14. F. J. McDonal et al., "Attenuation of Shear and Compressional Waves in Pierre Shale," Geophysics 23, 421 (1958).
15. B. F. Howell and D. Budenstein, "Energy Distribution in Explosion-Generated Seismic Pulses," Geophysics 20, 33 (1955).
16. J. E. White, Seismic Waves - Radiation, Transmission, and Attenuation (McGraw-Hill, New York, 1965).
17. D. V. Power, LRL, private communication, 11 December 1967.

Appendix A
Peak Motion Data

CONTENTS

Table AI. Peak motion data for site calibration events at LRL and LRL/MSU stations.[1]

Station	Component	Peak velocity (cm/sec)	Comments
		SC-1	
2NE Crest of dam	R (Radial)	1.65×10^{-3}	Maximum resultant occurred when R component was maximum. Particle motion approximately elliptical in the horizontal plane.
	T (Transverse)	0.92×10^{-3}	
	V (Vertical)	0.89×10^{-3}	
	Res. (Resultant)	1.67×10^{-3}	
3A-NE Base of dam	R	1.20×10^{-3}	First maximum was in the vertical-radial plane, and the second maximum (1.9 sec later) was in the horizontal plane.
	T	1.03×10^{-3}	
	V	1.38×10^{-3}	
	Res.		
	1st max.	1.44×10^{-3}	
	2nd max.	1.45×10^{-3}	
1NE	R	$>7 \times 10^{-3}$	Instrument recorders overdriven.
	T	$>8 \times 10^{-3}$	
	V	$>5 \times 10^{-3}$	
		SC-4	
1NE	R	6.6×10^{-3}	
	T	3.7×10^{-3}	
	V	5.4×10^{-3}	
2NE	R	0.75×10^{-3}	Motion was primarily in horizontal plane at maximum resultant.
	T	0.39×10^{-3}	
	V	0.45×10^{-3}	
	Res.	0.76×10^{-3}	
3B-NE	R	0.25×10^{-3}	Motion at maximum resultant was in vertical-radial plane. Signal-to-noise ratio for R and T components was about 2:1.
	T	0.29×10^{-3}	
	V	1.09×10^{-3}	
	Res.	1.09×10^{-3}	
		SC-2	
1NE	R	9.5×10^{-3}	
	T	7.4×10^{-3}	
	V	11.3×10^{-3}	
2NE	R	1.54×10^{-3}	Motion at maximum resultant was nearly elliptical in the horizontal plane. Maximum resultant was essentially due to a motion in the radial direction only.
	T	0.85×10^{-3}	
	V	0.80×10^{-3}	
	Res.	1.55×10^{-3}	

Table AI. (Continued)

Station	Component	Peak velocity (cm/sec)	Comments
		SC-2 (Continued)	
3A-NE	R	1.11×10^{-3}	Peak motion was due almost entirely to a vertical motion early in the wave train.
	T	0.91×10^{-3}	
	V	1.22×10^{-3}	
	Res.	1.22×10^{-3}	
		SC-3	
4W	R	9.56×10^{-2}	Peak resultant occurred at 0.15 sec after first motion. Resultant velocity exceeded 7×10^{-2} cm/sec eleven times. Vertical velocity exceeded 7×10^{-2} cm/sec nine times. Radial velocity exceeded 7×10^{-2} cm/sec twice. Motion was less than 10% of peak velocity at all times later than 11.88 sec after first motion.
	T	4.13×10^{-2}	
	V	13.97×10^{-2}	
	Res.	14.56×10^{-2}	
5W	R	1.47×10^{-2}	Peak resultant occurred at 0.34 sec after first motion. Resultant exceeded 10^{-2} cm/sec 28 times; radial, 10 times; transverse, 2 times; vertical 9 times.
	T	1.05×10^{-2}	
	V	1.88×10^{-2}	
	Res.	1.89×10^{-2}	
6W	R	0.32×10^{-2}	Peak resultant limits computed from ratios of resultant to maximum components for stations 4W and 5W.
	T	0.18×10^{-2}	
	V	0.34×10^{-2}	
	Res. (estimated)	$\sim 0.35 \times 10^{-2}$	
7W	R	0.13×10^{-2}	Vertical failed to operate properly; upper and lower limits for resultant value are estimated based upon ratios of component motions and resultants at other stations.
	V	—	
	Res.	$0.14 < R < 0.20$	

Table AII. Frequency content of signals for site calibration events at LRL and LRL/MSU stations.[1]

Station	Component	Event	Frequency of peak motion (Hz)	Predominant frequencies (Hz)	Arrival times of peak motion after first motion (sec)
1NE	R		3		~8
	T	SC-1	3	3 and 8	~9
	V		8		~1
	R		3		Too noisy to determine first motion.
	T	SC-4	2	2, 3 and 10	
	V		10		
	R		2.5		9
	T	SC-2	2.7	2.5 and 8	8.5
	V		8		1.5
2NE	R		2		19
	T	SC-1	2	2 and 8	16
	V		7		3
	Res.		2		3
	R		2		Very noisy records. Times unavailable.
	T	SC-4	2	2, 4 and 8	
	V		8		
	Res.		2		
	R		2		19
	T	SC-2	2	2 and 8	15
	V		8		3
	Res.		2		19
3A-NE	R		4		-30
	T	SC-1	2.5	2, 4 and 8	14
	V		8		1
	Res.		8		1
	R		4		4.5
	T	SC-2	2	2, 4 and 8	19.2
	V		8		3.0
	Res.		8		3.0
3B-NE	R		1.5 and 8		Record too noisy to determine first motion.
	T	SC-4	1.5	1.5 and 8	
	V		8		
	Res.		8		

Table AII. (Continued)

Station	Component	Event	Frequency of peak motion (Hz)	Predominant frequencies (Hz)	Arrival times of peak motion after first motion (sec)
4W	R	SC-3	4	2.5, 4 and 14	3.5
	T		4		4.0
	V		14		0.15
	Res.		14		0.15
5W	R	SC-3	3	3, 4 and 10	5.0
	T		4		5.0
	V		10		0.34
	Res.		10		0.34
6W	R	SC-3	2	2 and 10	13
	T		2		10
	V		10		2.5
7W	R	SC-3	2	2 and 6	18
	T		—		

Table AIII. Peak motion data at LRL intermediate range stations for Pre-Gondola I events.[1]

Station	Component	Peak velocity (cm/sec)	Error in signal	Comments
		Bravo		
2N (2B-N)	R	7.6×10^{-2}	10 ±%	Motion exceeded 0.7 × peak velocity on 6 separate half-cycles.
	T	3.40×10^{-2}	3	
	V	12.0×10^{-2}	11	
	Res.	12.9×10^{-2}	11	
3N	R	1.60×10^{-2}	—	Poor record since the level of the electronics was set to receive about 3 mm/sec.
	T	1.00×10^{-2}	—	
	V	1.25×10^{-2}	—	
	Res.	2.20×10^{-2}	—	
4N	R	2.07×10^{-3}	—	Early motions are not as distinct as at other stations; resultant motion exceeded 0.7 × peak velocity 13 times.
	T	1.42×10^{-3}	2	
	V	2.57×10^{-3}	5	
	Res.	3.06×10^{-3}	5	
5N	R	2.26 or 2.6×10^{-3}	—	Very high motions (the reason for this is not clear at this time). Two different recorders gave the two readings at left. Motion never exceeded 0.7 × peak velocity at any other time.
	T	1.3 or 1.49×10^{-3}	—	
	V	7.36 or 9.60×10^{-3}	—	
	Res.	7.37 or 9.70×10^{-3} (see Comments)	—	
6W	R	2.65×10^{-1}	—	Excellent record; resultant motion exceeded 0.7 × peak velocity on 12 half-cycles.
	T	1.63×10^{-1}	—	
	V	2.70×10^{-1}	—	
	Res.	3.07×10^{-1}	—	
		Charlie		
2N (2B-N)	R	7.5×10^{-2}	5	Motions exceeded 0.7 × peak velocity on only 2 half-cycles.
	T	2.8×10^{-2}	7	
	V	13.8×10^{-2}	7	
	Res.	14.6×10^{-2}	7	
		Delta		
2N (2B-N)	R	17.2×10^{-2}	—	Motions exceeded 0.7 × peak velocity on 6 half-cycles.
	T	7.2×10^{-2}	—	
	V	22.0×10^{-2}	—	
	Res.	24.5×10^{-2}		

Table AIII. (Continued)

Station	Component	Peak velocity (cm/sec)	Error in signal	Comments
		Alfa		
2N (2B-N)	R	11.0×10^{-2}	20	Motions exceeded 0.7 × peak velocity on 4 half-cycles.
	T	4.5×10^{-2}	16	
	V	19.4×10^{-2}	12	
	Res.	20.9×10^{-2}	12	

Table AIV. Frequency content of signals at LRL intermediate range stations for Pre-Gondola I events. [1]

Station	Event	Component	Frequency of peak motion (Hz)	Predominant frequencies (Hz)	Time of arrival of peak velocity after first motion (sec)
(2N)					
2B-N	Bravo	R	1.75	1.75, 5.5	12.4
		T	1.2	1.2	12.4
		V	4.5	1.5, 4.5	2.4
		Res.	—	—	2.4
	Alfa	R	6.0	1.5, 6.0	2.32
		T	2.0	2.0, 6.0	11.9
		V	5.0	1.5, 5.0	2.25
		Res.	—	—	2.25
	Charlie	R	1.5, 5.0	1.5, 5.0	3.2 and 11.2
		T	1.5	1.5, 5.0	12.8
		V	5.0	1.5, 5.0	3.1
		Res.	—	—	3.1
	Delta	R	1.75	1.75, 5.0	11.8
		T	1.75	1.75	13.5
		V	6.0	1.5, 6.0.	2.26
		Res.	—	—	2.34
3N[a]	Bravo	R	1.5	1.5	—
		T	1.5	1.5	—
		V	2.5	2.5	—
		Res.	—	—	—
4N	Bravo	R	3.0	0.75, 3.0	12.65
		T	3.0	0.75, 3.0	14.7
		V	2.5	0.75, 2.5	13.5
		Res	—	—	13.5
5N	Bravo	R	7.0	2, 7	5.48
		T	8.0	2, 6, 8	5.53
		V	8.0	3, 8	4.2
		Res.	—	—	4.2
6W	Bravo	R	1.65, 9.0	1.65, 9.0	1.34 and 5.44
		T	9.0	1.65, 4, 9	1.33
		V	1.75, 9.0	1.65, 9.0	0.31
		Res.	—	—	1.34

[a]Very low level signals due to low gain of recorder.

Table AV. Peak motion data for site calibration events at WES structures instrumentation stations.[2]

Station	Component	Peak velocity (cm/sec)	Frequency (Hz)
		SC-1	
1	V	1.39×10^{-3}	6.0
	R	0.79×10^{-3}	6.5
	T	1.04×10^{-3}	8.5
2	V	$0.83^{a} \times 10^{-3}$	6.2
	R	$1.27^{a} \times 10^{-3}$	21.0
	T	$0.88^{a} \times 10^{-3}$	23.0
3	V	0.57×10^{-3}	2.8
	R	0.23×10^{-3}	2.8
	T	0.25×10^{-3}	8.5
		SC-2	
1	V	1.01×10^{-3}	7.0
	R	0.76×10^{-3}	5.0
	T	0.98×10^{-3}	4.0
2[b]	V	$1.13^{a} \times 10^{-3}$	2.8
	R	—	—
	T	$0.54^{a} \times 10^{-3}$	3.5
3	V	0.28×10^{-3}	2.8
	R	0.15×10^{-3}	2.8
	T	0.12×10^{-3}	4.0
		SC-3	
1	V	1.21×10^{-3}	4.5
	R	0.87×10^{-3}	9.7
	T	1.63×10^{-3}	3.5
2[b]	V	$1.50^{a} \times 10^{-3}$	2.8
	R	—	—
	T	$0.55^{a} \times 10^{-3}$	3.5
3	V	0.55×10^{-3}	3.0
	R	0.25×10^{-3}	3.0
	T	0.32×10^{-3}	2.5

Table AV. (Continued)

Station	Component	Peak velocity (cm/sec)	Frequency (Hz)
		SC-4	
1	V	0.79×10^{-3}	3.5
	R	0.68×10^{-3}	4.0
	T	1.20×10^{-3}	4.0 and 8.5
2[b]	V	$0.85^{a} \times 10^{-3}$	6.5
	R	—	—
	T	$0.68^{a} \times 10^{-3}$	6.5
3	V	0.22×10^{-3}	2.8
	R	0.10×10^{-3}	8.5
	T	0.09×10^{-3}	10.0

[a]Background noise. Station 2 was located on Gate control shaft 3. At this station, background noise recorded just prior to each shot was of the same amplitude as that noted when the signal from the shot was present.

[b]Channel recording radial velocity at station 2 was lost after Shot SC-1 due to amplifier malfunction.

Table AVI. Peak motion data for Pre-Gondola I events at WES structures instrumentation stations.[2]

Station	Component	Peak velocity (cm/sec)	Frequency (Hz)
		Alfa	
1	V	2.6×10^{-2}	4.5
		2.6×10^{-2}	1.25
	R	1.9×10^{-2}	4.3
		2.6×10^{-2}	1.25
	T	3.3×10^{-2}	4.3
		4.2×10^{-2}	1.25
2	V	1.6×10^{-2}	4.3
	R	1.5×10^{-2}	4.3
	T	0.87×10^{-2}	4.3
3	V	1.5×10^{-2}	4.5
	R	0.75×10^{-2}	4.5
	T	0.62×10^{-2}	4.5
		Bravo	
1	V	2.9×10^{-2}	4.5
		2.5×10^{-2}	1.25
	R	2.0×10^{-2}	4.5
		2.3×10^{-2}	1.25
	T	2.9×10^{-2}	4.5
		3.6×10^{-2}	1.25
2	V	1.4×10^{-2}	3.5
	R	1.3×10^{-2}	3.5
	T	0.87×10^{-2}	3.5
3	V	—[a]	—
	R	—[a]	—
	T	—[a]	—
		Charlie	
1	V	2.8×10^{-2}	4.3
		2.9×10^{-2}	1.25
	R	1.9×10^{-2}	4.3
		2.7×10^{-2}	1.25
	T	2.5×10^{-2}	4.3
		4.2×10^{-2}	1.25
2	V	1.3×10^{-2}	4.3
	R	1.1×10^{-2}	4.3
	T	0.90×10^{-2}	4.3
3	V	1.1×10^{-2}	4.3
	R	—[b]	
	T	0.39×10^{-2}	4.3

Table AVI. (Continued)

Station	Component	Peak velocity (cm/sec)	Frequency (Hz)
		Delta	
1	V	3.4×10^{-2}	4.3
		2.6×10^{-2}	1.25
	R	2.3×10^{-2}	4.3
		3.6×10^{-2}	1.25
	T	2.8×10^{-2}	4.1
		5.3×10^{-2}	1.25
2	V	1.5×10^{-2}	4.3
	R	1.5×10^{-2}	4.5
	T	0.93×10^{-2}	4.5
3	V	1.3×10^{-2}	4.3
	R	0.82×10^{-2}	4.0
	T	0.51×10^{-2}	4.0

[a]Recordings of station 3 were lost due to amplifier power failure.

[b]Channel recording radial velocity at station 3 was lost due to broken wire.

Table AVII. Peak motion data for seismic decoupling experiment shots.

Shot	Station	Component	Peak velocity (cm/sec)	Approx. frequency (Hz)
SD1	LRL 6W	V	13.0×10^{-3}	10
			5.8×10^{-3}	2
		R	4.0×10^{-3}	7
			9.7×10^{-3}	3
		T	4.0×10^{-3}	3.5
			6.9×10^{-3}	3
SD2	LRL 6W	V	14.0×10^{-3}	10
			6.6×10^{-3}	2
		R	4.9×10^{-3}	7
			11.0×10^{-3}	3
		T	4.0×10^{-3}	3.5
			8.1×10^{-3}	3
SD1	LRL 2N	V	4.7×10^{-3}	10
			1.9×10^{-3}	1.7
		R	1.7×10^{-3}	9
			5.0×10^{-3}	2
		T	0.8×10^{-3}	9
			2.0×10^{-3}	2
SD2	LRL 2N	V	4.8×10^{-3}	10
			3.0×10^{-3}	1.7
		R	2.0×10^{-3}	8
			7.0×10^{-3}	2
		T	0.8×10^{-3}	10
			3.0×10^{-3}	2
SD1	WES 1	V	7.6×10^{-4}	4.5
			9.9×10^{-4}	1.25
		R	9.1×10^{-4}	4.5
			12.4×10^{-4}	1.25
		T	7.1×10^{-4}	4.5
			6.1×10^{-4}	1.25
SD2	WES 1	V	11.7×10^{-4}	4.5
			14.0×10^{-4}	1.25
		R	12.4×10^{-4}	4.5
			16.2×10^{-4}	1.25
		T	9.7×10^{-4}	4.5
			12.4×10^{-4}	1.25
SD1	WES 3	V	4.1×10^{-4}	4.5
			1.5×10^{-4}	1.25
		R	1.6×10^{-4}	4.5
			1.0×10^{-4}	1.25
		T	2.0×10^{-4}	4.5
			1.0×10^{-4}	1.25

Table AVII. (Continued)

Shot	Station	Component	Peak velocity (cm/sec)	Approx. frequency (Hz)
SD2	WES 3	V	5.1×10^{-4}	4.5
			1.8×10^{-4}	1.25
		R	2.0×10^{-4}	4.5
			1.6×10^{-4}	1.25
		T	2.3×10^{-4}	4.5
			1.3×10^{-4}	1.25
SD1	WES 4	V	5.3×10^{-4}	4.5
			1.8×10^{-4}	1.25
		R	4.3×10^{-4}	4.5
			1.5×10^{-4}	1.25
		T	2.8×10^{-4}	4.5
			1.5×10^{-4}	1.25
SD2	WES 4	V	6.9×10^{-4}	4.5
			2.0×10^{-4}	1.25
		R	5.1×10^{-4}	4.5
			1.8×10^{-4}	1.25
		T	3.0×10^{-4}	4.5
			1.8×10^{-4}	1.25

Note: Peak velocities from the 1000-lb seismic decoupling experiment shot were below the background vibration levels at WES stations 2 and 5.

Appendix B

Pre-Gondola Technical Reports

Title of Report	Agency	Author and/or Technical Program Officer	Report Number
Pre-Gondola -			
Seismic Site Calibration	NCG	M. K. Kurtz B. B. Redpath	PNE-1100
Site Selection Investigations	NCG/Omaha	H. A. Jack W. W. Dudley	PNE-1101
Pre-Gondola I -			
Technical Director's Summary Report	NCG	M. K. Kurtz et al.	PNE-1102
Geologic and Engineering Properties Investigations	NCG/Omaha	P. R. Fisher	PNE-1103
Close-in Ground Motion, Earth Stress, and Pore Pressure Measurements.	WES	J. D. Day et al.	PNE-1104
Intermediate Range Ground Motion	LRL	D. V. Power	PNE-1105
Structures Instrumentation	WES	R. F. Ballard	PNE-1106
Crater Studies: Crater Measurements	NCG	R. W. Harlan	PNE-1107 Part I
Surface Motion	NCG	W. G. Christopher	PNE-1107 Part II
Cloud Development Studies	NCG/LRL	W. C. Day R. F. Rohrer	PNE-1108
Close-in Displacement Studies	AFWL	C. J. Lemont	PNE-1109
Lidar Observations of Pre-Gondola I Clouds	SRI	J. W. Oblanas R. T. H. Collis	PNE-1110
Preshot Geophysical Measurements	LRL-N	R. T. Stearns J. T. Rambo	PNE-1111
Pre-Gondola II -			
Technical Director's Summary Report	NCG	W. C. Day/ M. K. Kurtz, Jr.	PNE-1112
Close-in Ground Motion and Earth Stress	WES	J. D. Day	PNE-1113
Engineering Properties Investigations	NCG	P. R. Fisher/ W. W. Dudley, Jr./ A. D. Frandsen	PNE-1114

Pre-Gondola II - (Continued)

Intermediate Range Ground Motion	LRL	D. Power	PNE-1115
Structures Instrumentation	WES	R. F. Ballard	PNE-1116
Crater Studies:			
Crater Measurements and Ejecta Studies	NCG	R. W. Harlan/ M. A. Novak	PNE-1117 Part I.
Ground Surface Motion	NCG	J. E. Lattery	PNE-1117 Part II.
Cloud Development Studies	NCG	W. C. Day	PNE-1118
Airborne LIDAR Observations		R. T. Collis J. Oblanas	PNE-1119
Survival of Simulated Pre-emplaced Charges	WES	J. D. Day	WES TR
Close-in Air Blast	BRL	J. Keefer	BRL TR

Distribution

LRL Internal Distribution

Michael M. May
R. Batzel
J. Gofman
H. L. Reynolds
C. H. Haussmann
J. Rosengren
D. Sewell
C. Van Atta
P. Molthrop
F. Eby
E. Goldberg
G. Higgins
J. Carothers
S. Fernbach
J. Hadley
J. Kane
B. Rubin
J. Kury
P. Stevenson
J. Bell
E. Hulse
W. Decker
W. Harford
G. Werth
M. Nordyke
F. Holzer
D. Power 2
H. Tewes
J. Toman 2
J. Knox
E. Teller, Berkeley
D. M. Wilkes, Berkeley
L. Crooks, Mercury
TID Berkeley
TID File 30

External Distribution

D. J. Convey
Department of Mines and Technical Surveys
Ottawa, Ontario, Canada

External Distribution (Continued)

G. W. Govier
Oil and Gas Conservation Board
Calgary, Alberta, Canada

R. Needham
LASA Data Center
Billings, Montana

U. S. Army Engineer Division
Lower Mississippi Valley
Vicksburg, Mississippi

U. S. Army Engineer District
Memphis, Tennessee

U. S. Army Engineer District
New Orleans, Louisiana

U. S. Army Engineer District
St. Louis, Missouri

U. S. Army Engineer District
Vicksburg, Mississippi

U. S. Army Engineer Division, Mediterranean
Leghorn, Italy

U. S. Army Liaison Detachment
New York, N. Y.

U. S. Army Engineer District, Gulf
Teheran, Iran

U. S. Army Engineer Division, Missouri River 2
Omaha, Nebraska

U. S. Army Engineer District
Kansas City, Missouri

U. S. Army Engineer District 2
Omaha, Nebraska

U. S. Army Engineer Division, New England
Waltham, Massachusetts

U. S. Army Engineer Division, North Atlantic
New York, N. Y.

U. S. Army Engineer District
Baltimore, Maryland

U. S. Army Engineer District
New York, N. Y.

U. S. Army Engineer District
Norfolk, Virginia

U. S. Army Engineer District
Philadelphia, Pennsylvania

External Distribution (Continued)

U.S. Army Engineer Division, North Central
Chicago, Illinois

U.S. Army Engineer District
Buffalo, New York

U.S. Army Engineer District
Chicago, Illinois

U.S. Army Engineer District
Detroit, Michigan

U.S. Army Engineer District
Rock Island, Illinois

U.S. Army Engineer District
St. Paul, Minnesota

U.S. Army Engineer District, Lake Survey
Detroit, Michigan

U.S. Army Engineer Division, North Pacific
Portland, Oregon

U.S. Army Engineer District
Portland, Oregon

U.S. Army Engineer District, Alaska
Anchorage, Alaska

U.S. Army Engineer District
Seattle, Washington

U.S. Army Engineer District
Walla Walla, Washington

U.S. Army Engineer Division, Ohio River
Cincinnati, Ohio

U.S. Army Engineer District
Huntington, West Virginia

U.S. Army Engineer District
Louisville, Kentucky

U.S. Army Engineer District
Nashville, Tennessee

U.S. Army Engineer District
Pittsburgh, Pennsylvania

U.S. Army Engineer Division, Pacific Ocean
Honolulu, Hawaii

U.S. Army Engineer District, Far East
San Francisco, California

U.S. Army Engineer District
Honolulu, Hawaii

External Distribution (Continued)

U.S. Army Engineer District, Okinawa
San Francisco, California

U.S. Army Engineer District, South Atlantic
Atlanta, Georgia

U.S. Army Engineer Division, Canaveral
Meritt Island, Florida

U.S. Army Engineer District
Charleston, South Carolina

U.S. Army Engineer District
Jacksonville, Florida

U.S. Army Engineer District
Mobile, Alabama

U.S. Army Engineer District
Savannah, Georgia

U.S. Army Engineer District
Wilmington, North Carolina

U.S. Army Engineer Division, South Pacific
San Francisco, California

U.S. Army Engineer District
Los Angeles, California

U.S. Army Engineer District
Sacramento, California

U.S. Army Engineer District
San Francisco, California

U.S. Army Engineer Division, Southwestern
Dallas, Texas

U.S. Army Engineer District
Albuquerque, New Mexico

U.S. Army Engineer District
Fort Worth, Texas

U.S. Army Engineer District
Galveston, Texas

U.S. Army Engineer District
Little Rock, Arkansas

U.S. Army Engineer District
Tulsa, Oklahoma

Mississippi River Commission
Vicksburg, Mississippi

Rivers and Harbors
Board of Engineers
Washington, D.C.

External Distribution (Continued)

Corps of Engineer Ballistic Missile Construction Office
Norton Air Force Base, California

U. S. Army Engineer Center
Ft. Belvoir, Virginia

U. S. Army Engineering School
Ft. Belvoir, Virginia

U. S. Army Engineer Reactors Group
Ft. Belvoir, Virginia

U. S. Army Engineer Training Center
Ft. Leonard Wood, Missouri

U. S. Coastal Engineering Research Board
Washington, D. C.

U. S. Army Engineer Nuclear Cratering Group 100
Livermore, California

TID-4500 Distribution, UC-35, Nuclear Explosions-Peaceful Applications 292

Printed in USA. Available from the Clearinghouse for Federal Scientific and Technical Information, National Bureau of Standards, U. S. Department of Commerce, Springfield, Virginia 22151
Price: Printed Copy ~~$3.00~~; Microfiche ~~$0.65~~.

WF/lm